The cytotoxic effects of polymer-coated quantum dots and restrictions for live cell applications.

Stefaan J. Soenen[1,2], Jo Demeester[1], Stefaan C. De Smedt[1,*] and Kevin Braeckmans[1,2]

[1]Lab of General Biochemistry and Physical Pharmacy, Faculty of Pharmaceutical Sciences, Ghent University, Harelbekestraat 72, B-9000 Gent, Belgium

[2]Centre for Nano- and Biophotonics, Ghent University, Harelbekestraat 72, B-9000 Gent, Belgium

* Corresponding author: Tel.: + 32 9 264 80 76

Fax: + 32 9 264 81 89

Email: Stefaan.DeSmedt@UGent.be

Abstract

The interest in the biomedical use of highly fluorescent and photostable nanoparticles such as quantum dots (QDots) is vastly increasing. One major hurdle that impedes QDot use in live cells and animals is their potential toxicity. Here, we employ a recently described multiparametric setup to determine the concentration at which common polymer-coated QDots become non-cytotoxic. We found that toxic effects are strongly related to the intracellular QDot amount that can be controlled by their specific surface coating. Using lysosomal buffer systems and proliferation-restricted cells, intracellular QDots were found to localize in endosomes, where they generate reactive oxygen species, interfere with cell cytoskeleton and leach free Cd^{2+} ions due to QDot dissolution, resulting in increased toxicity and impeded QDot fluorescence. Furthermore, we find that asymmetric partitioning of QDots upon recurrent cell division results in the sacrifice of heavily-loaded cells and a rapid loss of particles in live cells, limiting the use of currently available QDots for long-term imaging and defining the non-cytotoxic concentration as 10-fold lower than commonly used concentrations.

1. Introduction

Quantum dots (QDots) are semiconductor nanocrystals of typically 1-10 nm diameter that exhibit exceptional fluorescence properties such as high brightness, increased photostability and narrow emission spectra compared to common organic fluorophores [1-4]. These properties have led to a wide application of QDots as fluorescent probes for imaging of fixed cells and tissues [5]. In biomedical research, the use of QDots has also been suggested to enable long-term fluorescence microscopy of labeled cells, selective labeling and isolation of mixed cell populations or as contrast agents for *in vivo* fluorescence imaging [3,6]. An important application is the *in vitro* labeling of stem or immune cells with QDots followed by the subsequent transplantation of these cells, enabling their follow up by non-invasive fluorescence imaging and facilitating histological examinations. In order for the transplanted cells to remain functional, it is of utmost importance that the QDots do not interfere with normal cell homeostasis and physiology. As to date the toxic effects of QDots remain a matter of debate [7-12], the use of QDots for live cell applications remains limited. The difficulties in assessing the cytotoxic effects of QDots stem from several factors, such as the wide variation in cell types used, often including cancer cells, the use of core-only or core-shell particles of varying composition and surface coatings, large differences in incubation conditions and variability in types of assays performed, resulting in many ambiguous findings being reported [13,14].

It is generally accepted that core-shell particles are less toxic than core-only particles due to the protective role of the shell layer and that the surface coating of the QDots plays a crucial factor in cytotoxicity [14,15]. However, most studies only report on short term effects, where the acute cytotoxic potential of the QDots is studied, while the long-term effect of cell-internalized QDots remains scarcely addressed [16]. The long-term effects are however

crucial since the envisaged biomedical applications require the presence of QDots in the cells for many days. The present work makes use of a recently established multiparametric protocol according to which the cytotoxic effects of nanoparticles are studied using multiple cell types (C17.2 neural progenitor cells, primary human umbilical vein endothelial cells (HUVECs) and rat PC12 pheochromocytoma cells) [17]. In order to get a better insight into the effects of QDots on cultured cells, multiple parameters were studied, including: cell viability, generation of reactive oxygen species (ROS) and secondary ROS effects, cell cycle transition, intracellular QDot localization and concentration, cell morphology and cell functionality. Special emphasis is on the effect of the QDots after several days of intracellular localization as well as on examining intracellular QDot stability and its contribution to QDot cytotoxicity. Furthermore, the extensive panel of tests allows to define the QDot concentration at which no negative effects are observed.

2. Materials and methods

2.1. Nanoparticles.

The QDots used were 565 ITK-carboxyl and 565 ITK-amino PEG systems, which were supplied by Invitrogen, Inc. (Belgium), Both type of QDots are cadmium telluride/cadmium selenide (CdTe/CdSe) core and zinc sulphide (ZnS) shell particles encapsulated within a polymer. Although details about the proprietary surface coating are not provided by Invitrogen, the particles are both encapsulated in the same polymer type, with different surface groups, being carboxyl or amino-PEG groups. The particles were provided as 8 μM QDot solutions in 50 mM borate buffer, pH 8.3. The hydrodynamic diameter and ζ-potential of the QDots were measured using a Nanosizer instrument (Malvern, Worcestershire, UK). The particles were suspended in phosphate buffered saline (PBS: 10 mM; pH 7.0) after which the measurements were performed (12 cycles/run) in quadruplicate. The value for the

hydrodynamic diameter of the particles is obtained using the intensity scaling. Data are expressed as mean ± standard deviation (n=4). For the carboxy-QDots, the hydrodynamic diameter equaled 15.6 ± 2.1 nm (polydispersity index: 0.163) and the ζ-potential was -23.1 ± 4.5 mV where PEG-QDots had a hydrodynamic diameter of 38.1 ± 4.2 nm (polydispersity index: 0.156) and a ζ-potential of 2.5 ± 3.1 mV, where the larger size of the PEG-QDots can be attributed to the presence of the PEG chains.

2.2. Cell culture.

C17.2 neural progenitor cells and PC12 cells are maintained in high glucose Dulbecco's Modified Eagle's Medium (DMEM), supplemented with 10% fetal bovine serum, 5% horse serum, 2 mM L-Glutamine and 1% Penicillin/Streptomycin (Gibco, Invitrogen, Merelbeke, Belgium). Cells were maintained in a humidified atmosphere at 5% CO_2 and fresh medium was given every other day. C17.2 cells were passaged (1/10) when reaching 90% confluency. PC12 cells were grown in 25 cm² cell culture flasks (Corning, Amsterdam, The Netherlands) which were coated with collagen (rat tail collagen type I, Invitrogen, Belgium) and passaged (1/5) when growing in small clumps (approximately 5 cells/clump and reaching 70-80% confluency). Fresh medium was given every other day. To establish non-proliferating cell populations, cells were exposed with 60 µM Apigenin (Sigma-Aldrich, Bornem, Belgium) together with the QDot exposure. After removal of the medium, fresh media containing 60 µM Apigenin was used, where media were replaced for 50% every other day with fresh Apigenin-containing medium for the duration of the experiments. Under these conditions, cell death was found to be minimal and cell proliferation was reduced to approximately 9% of the normal value. Furthermore, removal of the medium with normal cell culture medium not containing any Apigenin resulted in a recovery of cell proliferation to near-control levels after approximately three days.

Primary human umbilical vein endothelial cells (HUVECs) were kindly provided by Dr. Aldo Ferrari (ETH Zurich, Switzerland). For cultivation, cells were kept in 75 cm^2 cell culture flasks (Corning, Amsterdam, The Netherlands) which were coated with collagen (rat tail collagen type I, Invitrogen, Belgium) prior to cell seeding. The cells were maintained in endothelial cell basal growth medium and growth supplement (Cell Applications, Tebu-Bio, Le Perray en Yvelines, France) and passaged (1/5) when reaching 80-90% confluency. Every other day, fresh medium was given. To establish non-proliferating HUVEC cultures, cells were given endothelial cell serum-free defined medium (Cell Applications, Tebu-Bio, Le Perray en Yvelines, France) when reaching high levels of confluency. Confluent HUVEC monolayers could then be maintained for at least one week without any observable signs of cell death.

2.3. Cell-nanoparticle interaction studies.

A full methodology of all protocols can be found in the Supplementary information that accompanies this article.

3. Results and Discussion

3.1. Cell uptake and intracellular localization of QDots.

In the present work, two types of QDots as provided by a major commercial supplier (Invitrogen, Inc.) that have been frequently used for cell labeling purposes were tested. The QDots were 565 ITK-carboxyl and 565 ITK-amino PEG particles that are CdTe/CdSe-ZnS core-shell dots encapsulated in a polymer coating containing either carboxyl groups or amino-terminal PEG chains on their surface. In terms of cellular uptake, co-incubation of the C17.2 cells with 15 nM QDots and the green lipophilic dye DiO resulted in a clear colocalization of both types of red QDots and green vesicles, likely endosomes, as shown by confocal laser

scanning microscopy (**Figure 1A,B; Supplementary Figure S1**). Although both types of QDots exhibited a similar extent of endosomal colocalization, a large difference in cellular uptake levels was observed for both. This was confirmed by calculating the number of QDot clusters per cell, (**Figure 1C**) which was much higher for carboxy-QDots than for PEG-QDots at identical concentrations. The total number of QDots per cell showed a similar trend, where carboxy-QDots were internalized by the cells approximately 5 times more than PEG-QDots (**Figure 1D**). Interestingly, the number of QDots per vesicle appeared to be limited and a further increase of the intracellular amount of QDots appeared to be due to a higher number of QDot-containing endosomes (**Supplementary Figure S2A**). Also, the cellular uptake efficiency of the QDots, defined as the ratio of cell-associated QDots over the number of QDots in the original incubation medium, decreases for increasing QDot concentrations, hinting at a saturable uptake mechanism (**Supplementary Figure S2B**). Similar uptake levels were also reached in the HUVEC and PC12 cells (**Supplementary Figure S3**).

3.2. Effects of QDots on cell viability and oxidative stress.

Acute cytotoxic effects for all cell types were only observed for carboxy-QDots at 20 nM (**Figure 2A, Supplementary Figure S4**), likely as a result of the higher cellular uptake levels of these particles. Besides acute cytotoxicity, the generation of ROS has been described to play an important role in the toxicological profile of nanomaterials [18,19]. Here, the carboxy-QDots resulted in a concentration-dependent increase in ROS levels, whereas the PEG-QDots had only minimal effects (**Figure 2B**), which is not surprising since they are taken up much less. The increase in ROS was further found to be only transient, where levels dropped back to near control levels after two days (data not shown). Elevated ROS levels can also lead to secondary effects, as shown for the 20 nM carboxy-QDots that result in

significant elevations of damaged mitochondria, elevated calcium levels and even DNA damage (**Supplementary Figure S5**). The transient ROS elevation may be due to a continuous proliferation of the cells, which results in an exponential dilution of the cellular QDot levels. To circumvent this, C17.2 cells were incubated with 60 μM Apigenin resulting in a block in cell cycle progression (See Supporting Materials and Methods). To investigate ROS levels, C17.2 cells were incubated with the QDots and subsequently kept in culture without proliferating. Under these conditions, all types of QDots generated higher ROS levels as time progressed (**Figure 2C, Supplementary Figure S6**). Clearly, these data show that prolonged intracellular localization of the particles results in long-term and elevated stress levels.

3.3. Effects of intracellular QDot degradation.

To further study the effects of intracellular QDots, the release of toxic Cd^{2+} from the QDots was studied using three buffer systems with pH values of 7, 5 and 4, respectively, as described previously for iron oxide particle degradation [20]. **Figure 2D** clearly shows a time- and pH-dependent release of Cd^{2+}, the extent of which is similar for both types of QDots. Similarly, at lower pH, the QDot fluorescence intensity decreased, also as a function of time, possibly due to particle degradation (**Supplementary Figure S7**). Using proliferation-deficient cells, intracellular Cd^{2+} release was also found to increase in cells with time, being maximal for carboxy-QDots due to the higher intracellular particle levels (**Figure 2E, Supplementary Figure S8**) that correlated with an increased reduction in cell viability (**Supplementary Figure S9**). Although the generation of ROS can be reduced by co-exposure of C17.2 cells to 5 mM N-acetyl-cysteine (NAC), this led to only a partial recovery of cell viability, indicating the occurrence of other toxic effects. The intracellular degradation of the polymer-coated QDots in time has been clearly demonstrated and compromises QDot utility. Thus far, QDot degradation has only been studied scarcely and mostly for core-only particles,[21] using

extreme pH conditions,[15] aged particles[22] or chelating agents[23] resulting in chemical transformations. Recently, intracellular biothiols were described to degrade QDot monolayers, compromising their function.[16] Here, we have shown that commonly used polymer-coated QDots are not optimally designed for long use in the degradative endosomal environment as at later time points, especially in the case of slow or non-proliferating cells the cytotoxic effects of the particles further increase with time.

3.4. Effects of QDots on cell functionality at sub-toxic levels.

Next, the cellular effects of QDots were studied in more detail, using only those concentrations that did not evoke any acute toxicity. QDots were shown to result in clear deformations of cell morphology at 3 days after particle exposure, showing maximal deformations for carboxy-QDots at 10 nM (**Figure 3**). Similarly, at these particle concentrations, cells also showed affected spreading (**Figure 3, Supplementary Figure S10**) and were slightly inhibited in their proliferation and cell cycle progression (**Supplementary Figure S11**) which is in line with earlier reports on iron oxide particles [24,25]. To further study the time-dependent effects of QDots at non-toxic concentrations (carboxy-QDots at 5 nM and PEG-amine QDots at 10 nM), we employed the PC12 neurite outgrowth assay, a rapid and quantitative model to investigate cell functionality [26]. During the 3 day exposure of the PC12 cells to nerve growth factor, the cells proliferate only minimally, making it an excellent tool to study the effect of the particles after several days post exposure. **Figure 4** clearly shows a significant reduction in neurite outgrowth for PC12 cells treated with higher concentrations of either carboxy- or PEG-QDots, the safe levels of QDots for cell labeling appears to be 1 nM and 5 nM, respectively. Although the concentration of PEG-particles is higher, the lower cellular uptake efficiency and higher concentration needed to achieve similar intracellular concentrations also results in higher initial ROS and Cd^{2+} levels (**see Figure 2E and Supplementary Figure S6A+D**), making the carboxy-QDots best suited for

cell labeling. In a final part, the long-term follow up of cells labeled with the QDots at the non-toxic concentration was evaluated. **Figure 5** shows a clear asymmetric transfer of particles upon subsequent cell divisions, which is in line with several recent reports [27,28]. After 6 cell doublings, most cells treated with 1 nM of particles either contain little to no particles and are hardly detectable whereas some cells contain high levels of QDots (**Supplementary Figure S12**). Interestingly, the cells containing high levels of particles were found to be in a slow proliferating state and also displayed clear nuclear condensation, a potential sign of cell death. These events indicate that some cells are indeed sacrificed by containing high levels of particles while the majority of the cell population is actively proliferating but no longer contains any detectable amount of particles. When cells are incubated with 0.5 nM carboxy-QDots, no toxic effects were observed, but the rapid dilution of the particles rendered them detectable for only 4 cell doublings.

4. Conclusions.

The present work shows that common polymer-coated QDots do not appear to be optimally suited for long-term use when located in the degradative endosomal environment. Intraendosomal QDot degradation affects both cell and particle functionality. Concentrations at which no effects can be observed are quite low (commonly used concentrations for cell labeling are in the 2-20 nM range) and do not appear to be sufficient to allow long-term cell visualization. These data further show that the polymer-coated QDots studied here are not well suited for use in proliferation restricted cells, such as most cells from the human body. We would hypothesize that cells loaded with these QDots at higher concentrations and showing clear QDot levels at later time points either *in vitro* or *in vivo* likely indicate non-proliferating and possibly damaged cells, that may form a serious danger to the autologous host cells. More in-depth toxicological assays are necessary and nanoparticle effects should be

studied more at later time points. Toxicity data should also be coupled to functional (= intracellular) nanoparticle concentrations as the application of novel coatings that reduce both toxicity and cellular nanoparticle levels are functionally less relevant. Emphasis should therefore focus on optimizing QDot coatings that are more resistant against endosomal degradation. Alternatively it could be worthwhile to investigate the toxic effects of QDots that are delivered directly into the cytoplasm, as suggested for Qtracker particles.

Acknowledgements.

SJS is a post-doctoral fellow from the FWO-Vlaanderen. Financial support from the FWO-Vlaanderen (Krediet aan Navorsers to SJS) and the UGent consortium NB Photonics are gratefully acknowledged.

Appendix. Supplementary data

Supplementary data related to this article can be found online at …

Figure legends.

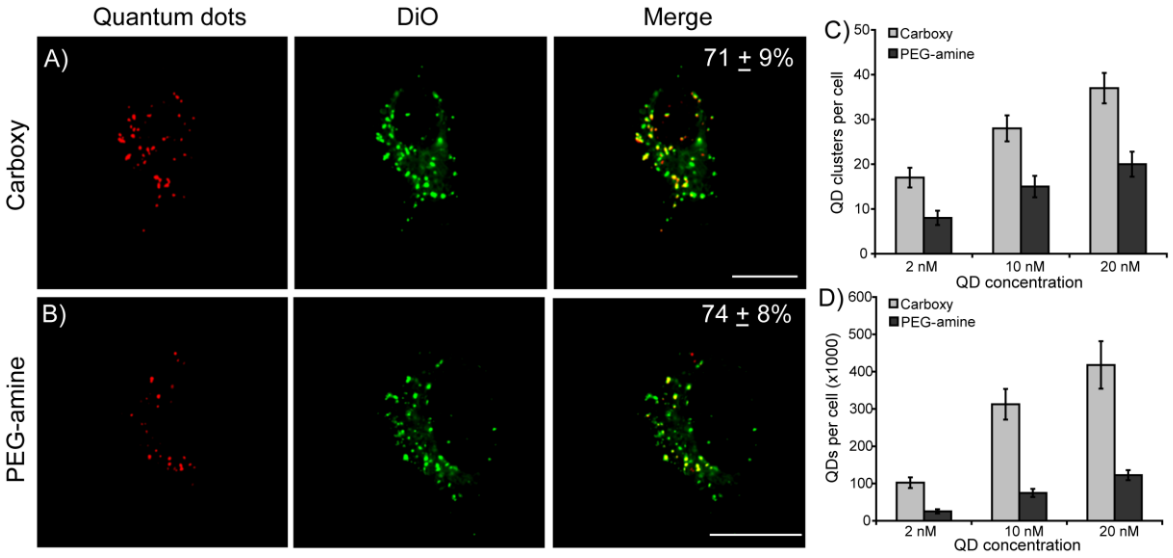

Figure 1. Cellular uptake of QDots. **A,B)** Representative confocal images of C17.2 neural progenitor cells incubated with 15 nM **(A)** carboxy- or **(B)** PEG-amine QDots (left column: red) for 30 min in the presence of the lipophilic dye DiO (middle column: green) that stains endosomal structures. A merged image of both the QDots and the DiO positive endosomes is shown in the right column where the percentage of colocalization of both QDots and DiO positive endosomes is shown in the top right corner, indicating a clear colocalization of both types of QDots and endosomal structures. Scale bars: 25 µm. **C)** The number of QDot clusters per cell as quantified from the microscopy images. **(D)** The total number of QDots per C17.2 cell as a function of the QDot concentration for both carboxy (light grey)- and PEG-amine QDots (dark grey) as quantified by measuring total fluorescence intensity levels (see Supporting Materials and Methods section). Data are shown as mean ± SEM (n = 4) and indicate a higher cellular internalization of carboxy-QDots over PEG-amine QDots.

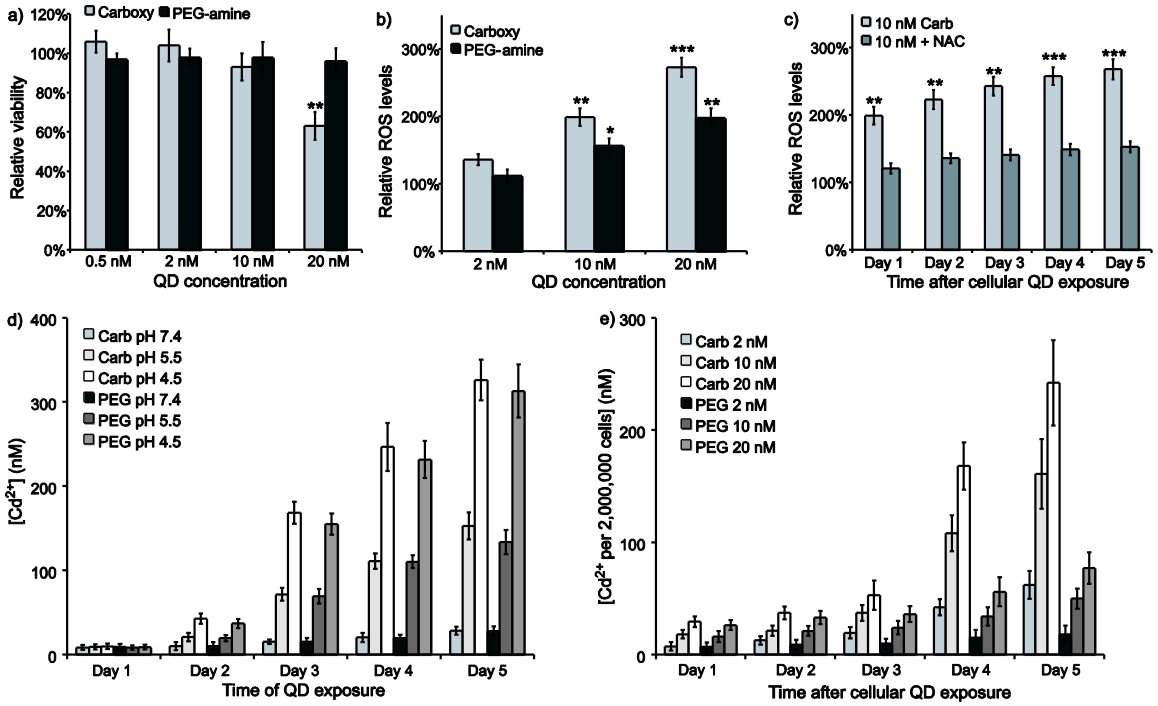

Figure 2. Evaluation of QDot toxicity and pH-dependent degradation. **A)** Viability of C17.2 cells and **B)** levels of reactive oxygen species (ROS) in C17.2 cells as a function of QDot concentration for both carboxy- and PEG-amine QDots after 24 h incubation. Data are represented as mean ± SEM (n = 8) and expressed as relative to untreated control cells, showing acute cytotoxic effects for carboxy-QDots at 20 nM and a clear concentration-dependent induction of ROS, that is most pronounced for carboxy-QDots. **C)** Levels of ROS in non-proliferating C17.2 cells exposed to 10 nM carboxy-QDots for 24 h and subsequently analyzed for ROS after 1, 2, 3, 4 or 5 days of additional culture showing a clear increase in cellular ROS levels. Cellular ROS levels could be reduced by co-exposure of C17.2 cells to 5 mM N-acetyl-cysteine (NAC), a potent free radical scavenger. Data are expressed as mean ± SEM (n = 8) against 60 µM Apigenin-treated control cells. **(A-C)** The degree of statistical significance of treated samples versus control samples is indicated when appropriate (**: $p < 0.01$; ***: $p < 0.001$). **D)** Levels of free Cd^{2+} in suspensions of either carboxy- or PEG-amine QDots at various pH values (7.4, 5.5, 4.5) as a function of time showing a clear pH-mediated

degradation of either type of QDot and similar associated Cd^{2+} release profiles. Data are expressed as mean ± SEM (n = 3). **E)** Levels of free Cd^{2+} in C17.2 cells exposed to either carboxy- or PEG-amine QDots for 24 h and subsequently kept in non-proliferating state after which the cellular Cd^{2+} levels are measured after 1, 2, 3, 4 and 5 days. The data are expressed as mean ± SEM (n = 3) and show a clear time-dependent increase in cellular Cd^{2+} levels, being more pronounced for the carboxy-QDots, which is in line with their much higher cellular uptake efficiency.

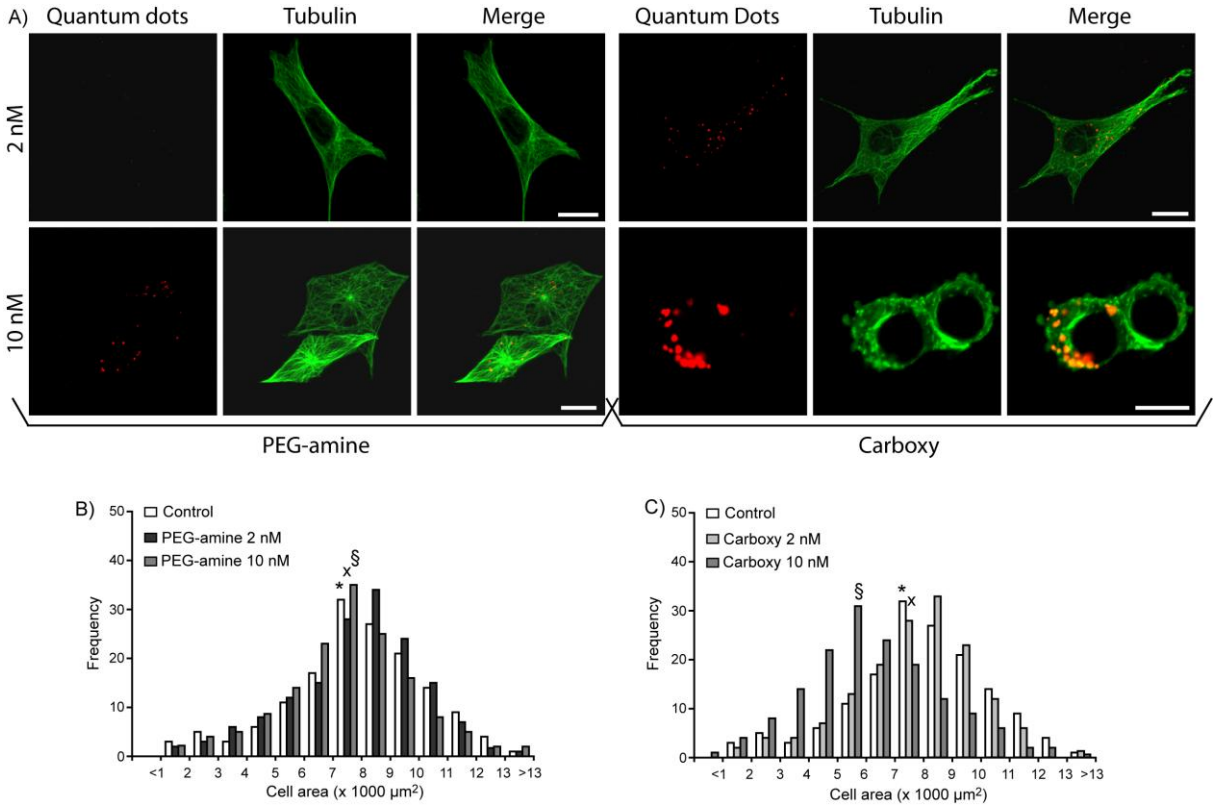

Figure 3. QDot induced cellular morphology defects: A) Representative confocal images of HUVEC cells exposed for 24 h to either PEG-amine (left panel)- or carboxy-QDots (right panel) at 2 nM (top row) or 10 nM (bottom row). After QDot exposure (red, left column) HUVEC cells were kept in culture for 3 more days after which they were immunostained for α-tubulin (green, middle column). The right column shows a merged image of both QDots and α-tubulin cytoskeleton. Scale bars: 30 µm. **B,C)** Histograms representing the cell area

distribution of HUVECs exposed to **(B)** PEG-amine QDots or **(C)** carboxy-QDots for 24 h and stained after 3 additional days of culture. The average cell areas are indicated with * for control cells, x for 2 nM-treated cells and § for 10 nM-treated cells. These data show a clear shift in cell area distribution of HUVECs exposed to 10 nM carboxy-QDots, likely due to the higher intracellular QDot levels and associated toxicity.

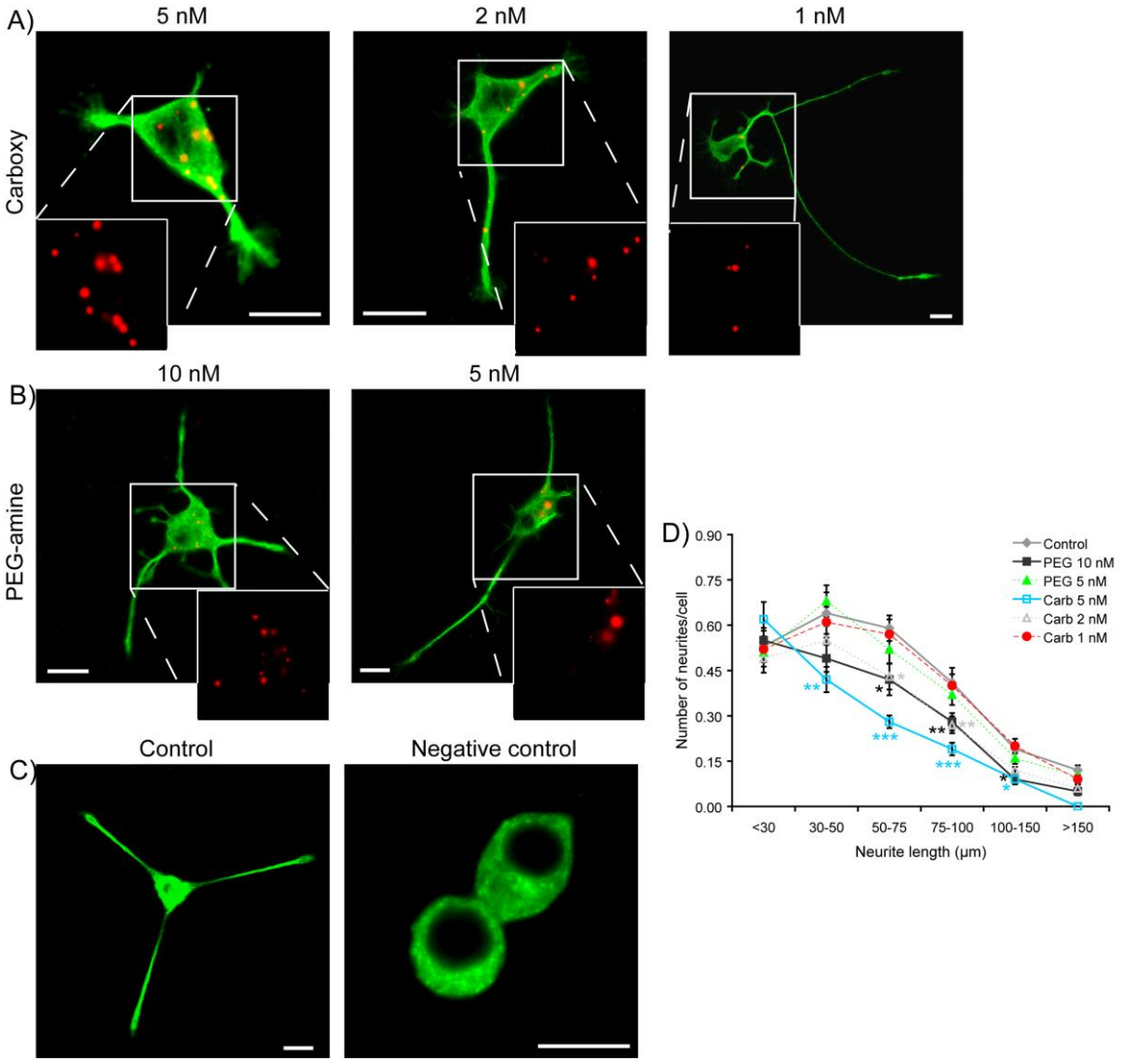

Figure 4. Effect of QDots on cell functionality. A-C) Representative confocal images of PC12 cells exposed to **(A)** carboxy-QDots, **(B)** PEG-amine QDots for 24 h or **(C)** not exposed to any QDots. **(A,B)** Following QDot exposure, the PC12 cells were exposed to nerve growth factor (NGF; 100 ng/ml) for 3 days that induces the outgrowth of neurites, after which the

cells were immunostained for α-tubulin. **(C)** Control cells were also stimulated with NGF for 3 days at 100 ng/ml, negative controls were kept in NGF-deprived medium for 3 days. The images show both α-tubulin staining (green) and cell-associated QDots (red). **(A,B)** The area indicated by the white rectangle is magnified at the bottom of the image, showing only the QDot fluorescence. Scale bars: 25 µm. **D)** The number of neurites of a certain length per cell after 3 days of NGF exposure for control cells or cells exposed to 5, 2 or 1 nM of carboxy-QDots or 10 or 5 nM of PEG-amine QDots. When appropriate, the degree of significance is given when compared with untreated control cells (*: $p < 0.05$; **: $p < 0.01$; ***: $p < 0.001$). These data indicate a clear concentration-dependent inhibition of cell functionality upon QDot exposure, finally reaching NOAELs when similar intracellular QDot levels are reached, being: 1 nM for carboxy-QDots and 5 nM for PEG-amine QDots.

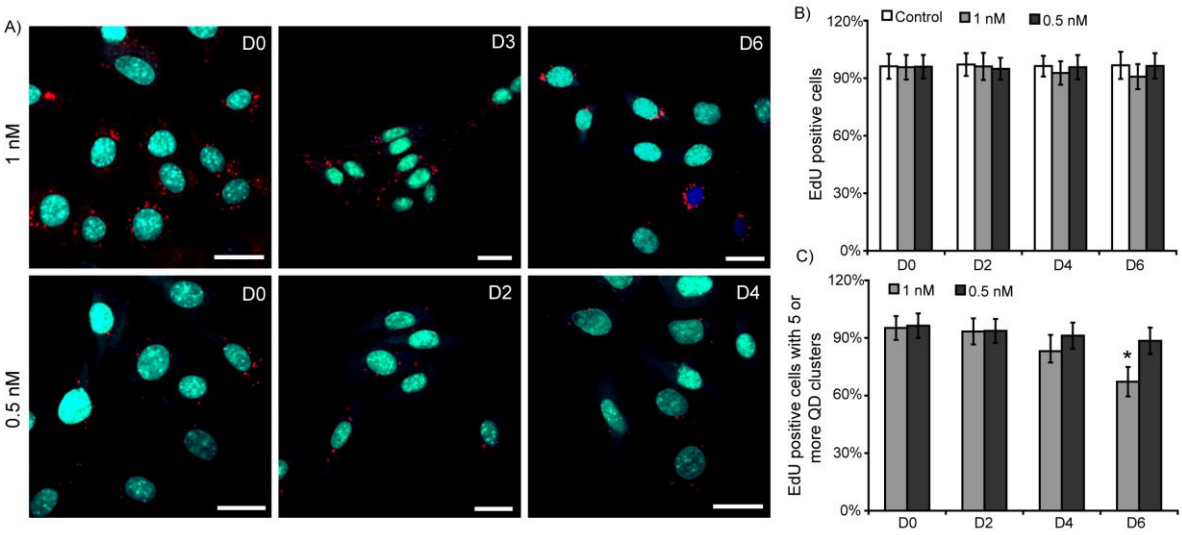

Figure 5. Effect of QDots upon concurrent cell division. A) Representative fluorescence images of C17.2 cells exposed to 1 nM (top row) or 0.5 nM (bottom row) carboxy-QDots for 24 h, after which the cells were kept in culture. The images shown are taken immediately after QDot exposure (D0) or after 2 (D2), 3 (D3), 4 (D4) or 6 (D6) average cell doubling times. 15 h prior to imaging, cells were further incubated with 10 µM EdU, a thymidine-analogue that

is incorporated in the nuclear DNA when proliferating cells progress through the S-phase of mitosis. The images show QDots (red), EdU-staining (green) and DAPI nuclear counterstaining (blue). Scale bars: 20 µm. The images show a clear asymmetric distribution of QDot clusters through concurrent cell division. Due to this, many cells contain only limited numbers of QDots after multiple cell divisions, impeding long term follow-up. Several cells acquire higher numbers of QDots, which appears to result in clear cytotoxic effects as shown by the impeded cell cycle progression and nuclear condensation. **B,C)** The percentage of EdU-positive cells for **B)** control cells or cells incubated with 1 nM or 0.5 nM carboxy-QDots for 24 h after 0, 2, 4 and 6 average cell doubling times or **C)** for cells having 5 or more QDot clusters per cell. When appropriate, differences compared with untreated control cells are indicated (*: $p < 0.05$). The data are expressed as mean $\pm$ SEM ($n = 3$) and indicate that the loss of cell proliferation is negligible in the overall cell population due to the vast increase in cells containing little numbers of QDots. However, when only selecting cells containing significant numbers of QDots, significant inhibition of cell cycle progression can be observed, highlighting the importance of careful cellular analysis on the single cell level. Please note that the lack of effect for cells exposed to 0.5 nM carboxy-QDots, even when reaching significant levels of QDot clusters is due to the smaller overall size of the clusters and thus the lower cellular QDot levels.

References

[1] Medintz IL, Uyeda HT, Goldman ER, Mattoussi H. Quantum dot bioconjugates for imaging, labelling and sensing. Nat Mater 2005;4:435-46.

[2] Michalet X, Pinaud FF, Bentolila LA, Tsay JM, Doose S, Li JJ, et al. Quantum dots for live cells, in vivo imaging, and diagnostics. Science 2005;307:538-44.

[3] Chan WC, Nie S. Quantum dot bioconjugates for ultrasensitive nonisotopic detection. Science 1998;281:2016-8.

[4] Yin Y, Alivisatos AP. Colloidal nanocrystal synthesis and the organic-inorganic interface. Nature 2005;437:664-70.

[5] Wu X, Liu H, Liu J, Haley KN, Treadway JA, Larson JP, et al. Immunofluorescent labeling of cancer marker Her2 and other cellular targets with semiconductor quantum dots. Nat Biotechnol 2003;21:41-6.

[6] Rivera-Gil P, Yang F, Thomas H, Li L, Terfort A, Parak WJ. Development of an assay based on cell counting with quantum dot labels for comparing cell adhesion within cocultures. Nano Today 2011;6:20-7.

[7] Chen N, He Y, Su Y, Li X, Huang Q, Wang H, et al. The cytotoxicity of cadmium-based quantum dots. Biomaterials 2011;33:1238-44.

[8] Qu Y, Li W, Zhou Y, Liu X, Zhang L, Wang L, et al. Full assessment of fate and physiological behavior of quantum dots utilizing Caenorhabditis elegans as a model organism. Nano Lett 2011;11:3174-83.

[9] Kirchner C, Liedl T, Kudera S, Pellegrino T, Javier AM, Gaub HE, et al. Cytotoxicity of colloidal CdSe and CdSe/ZnS nanoparticles. Nano Lett 2005;5:331-8.

[10] Choi HS, Liu W, Misra P, Tanaka E, Zimmer JP, Itty Ipe B, et al. Renal clearance of quantum dots. Nat Biotechnol 2007;25:1165-70.

[11] Bottrill M, Green M. Some aspects of quantum dot toxicity. Chem Commun 2011;47:7039-50.

[12] Hardman R. A toxicologic review of quantum dots: Toxicity depends on physicochemical and environmental factors. Environ Health Persp 2006;114:165-72.

[13] Zhang T, Stilwell JL, Gerion D, Ding L, Elboudwarej O, Cooke PA, et al. Cellular effect of high doses of silica-coated quantum dot profiled with high throughput gene expression analysis and high content cellomics measurements. Nano Lett 2006;6:800-8.

[14] Choi AO, Cho SJ, Desbarats J, Lovric J, Maysinger D. Quantum dot-induced cell death involves Fas upregulation and lipid peroxidation in human neuroblastoma cells. J Nanobiotechnology 2007;5:1.

[15] Mahendra S, Zhu HG, Colvin VL, Alvarez PJ. Quantum dot weathering results in microbial toxicity. Environ Sci Technol 2008;42:9424-30.

[16] Zhu ZJ, Yeh YC, Tang R, Yan B, Tamayo J, Vachet RW, et al. Stability of quantum dots in live cells. Nat Chem 2011;3:963-8.

[17] Soenen SJ, Rivera Gil P, Montenegro J-M, Parak WJ, De Smedt SC, Braeckmans K. Cellular toxicity of inorganic nanoparticles: Common aspects and guidelines for improved nanotoxicity evaluation. Nano Today 2011;6:446-465.

[18] Nel A, Xia T, Madler L, Li N. Toxic potential of materials at the nanolevel. Science 2006;311:622-7.

[19] Nel AE, Madler L, Velegol D, Xia T, Hoek EMV, Somasundaran P, et al. Understanding biophysicochemical interactions at the nano-bio interface. Nat Mater 2009;8:543-57.

[20] Soenen SJ, Himmelreich U, Nuytten N, Pisanic TR, 2nd, Ferrari A, De Cuyper M. Intracellular nanoparticle coating stability determines nanoparticle diagnostics efficacy and cell functionality. Small 2010;6:2136-45.

[21] Cho SJ, Maysinger D, Jain M, Roder B, Hackbarth S, Winnik FM. Long-term exposure to CdTe quantum dots causes functional impairments in live cells. Langmuir 2007;23:1974-80.

[22] Gagne F, Maysinger D, Andre C, Blaise C. Cytotoxicity of aged cadmium-telluride quantum dots to rainbow trout hepatocytes. Nanotoxicology 2008;2:113-20.

[23] Navarro DA, Banerjee S, Watson DF, Aga DS. Differences in soil mobility and degradability between water-dispersible CdSe and CdSe/ZnS quantum dots. Environ Sci Technol 2011;45:6343-9.

[24] Soenen SJ, Nuytten N, De Meyer SF, De Smedt SC, De Cuyper M. High intracellular iron oxide nanoparticle concentrations affect cellular cytoskeleton and focal adhesion kinase-mediated signaling. Small 2010;6:832-42.

[25] Soenen SJ, Himmelreich U, Nuytten N, De Cuyper M. Cytotoxic effect of iron oxide nanoparticles and implications for safety in cell labeling. Biomaterials 2011;32:195-205.

[26] Pisanic TR, Blackwell JD, Shubayev VI, Finones RR, Jin S. Nanotoxicity of iron oxide nanoparticle internalization in growing neurons. Biomaterials 2007;28:2572-81.

[27] Errington RJ, Brown MR, Silvestre OF, Njoh KL, Chappell SC, Khan IA, et al. Single cell nanoparticle tracking to model cell cycle dynamics and compartmental inheritance. Cell Cycle 2010;9:121-30.

[28] Summers HD, Rees P, Holton MD, Brown MR, Chappell SC, Smith PJ, et al. Statistical analysis of nanoparticle dosing in a dynamic cellular system. Nat Nanotechnol 2011;6:170-4.

The cytotoxic effects of quantum dots and restrictions for live cell applications.

Stefaan J. Soenen[1,2], Jo Demeester[1], Stefaan C. De Smedt[1,*] and Kevin Braeckmans[1,2]

[1]Lab of General Biochemistry and Physical Pharmacy, Faculty of Pharmaceutical Sciences, Ghent University, Harelbekestraat 72, B-9000 Gent, Belgium

[2]Centre for Nano- and Biophotonics, Ghent University, Harelbekestraat 72, B-9000 Gent, Belgium

* Corresponding author: Tel.: + 32 9 264 80 76

Fax: + 32 9 264 81 89

Email: Stefaan.DeSmedt@UGent.be

Supplementary information.

Supplementary figures.

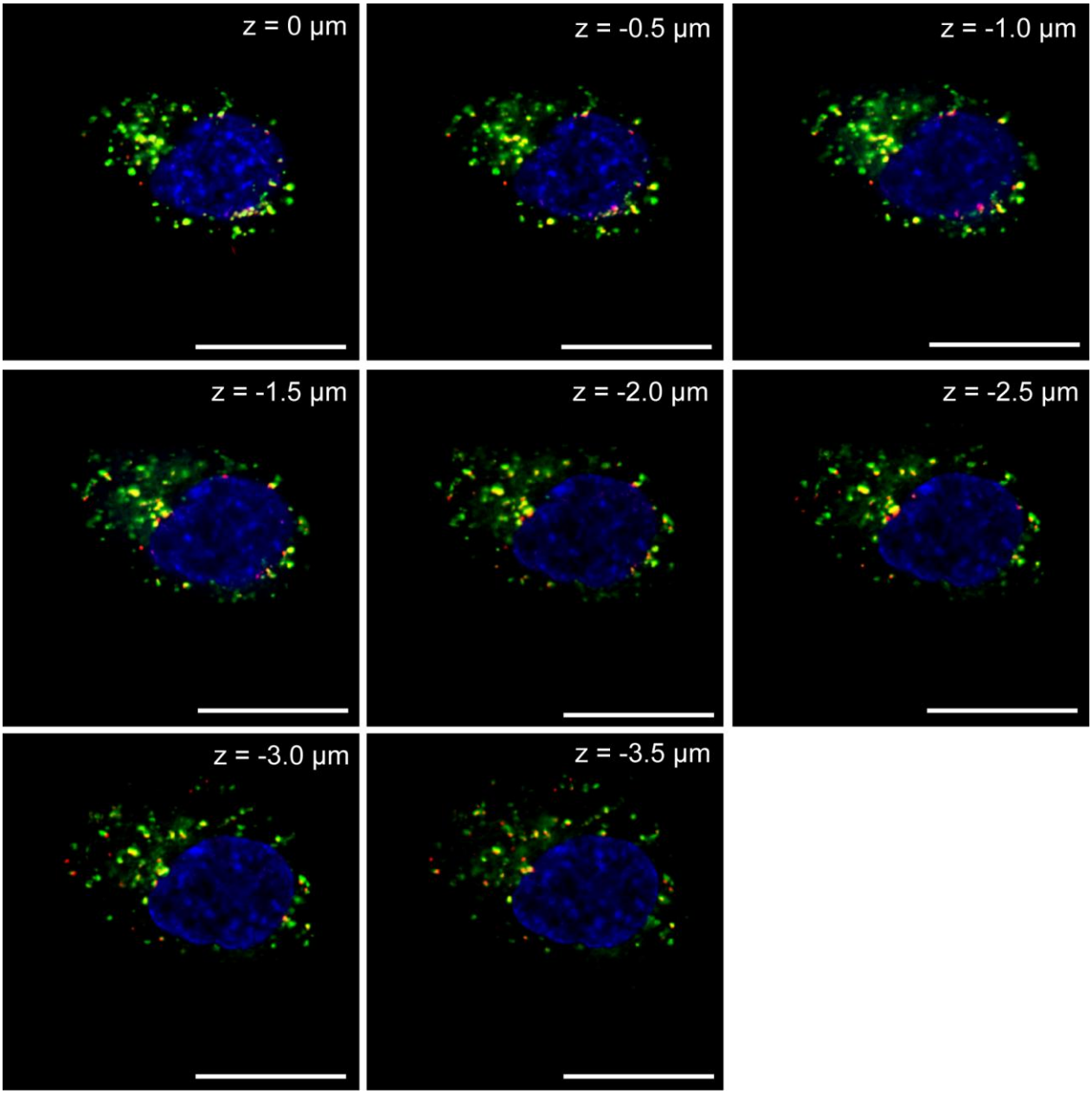

Supplementary Figure S1. Endosomal localization of carboxy-QDots. Representative confocal images of a single C17.2 cell exposed to 15 nM carboxy-QDots (red) and DiO (green) for 30 min. The cell nucleus is counterstained using DAPI (blue). A series of 8 images are shown of the same cell for different confocal slices going from the top towards the bottom of the cell. Each image corresponds to a displacement of 0.5 µm of the objective lens further along the Z-axis. Scale bar: 25 µm.

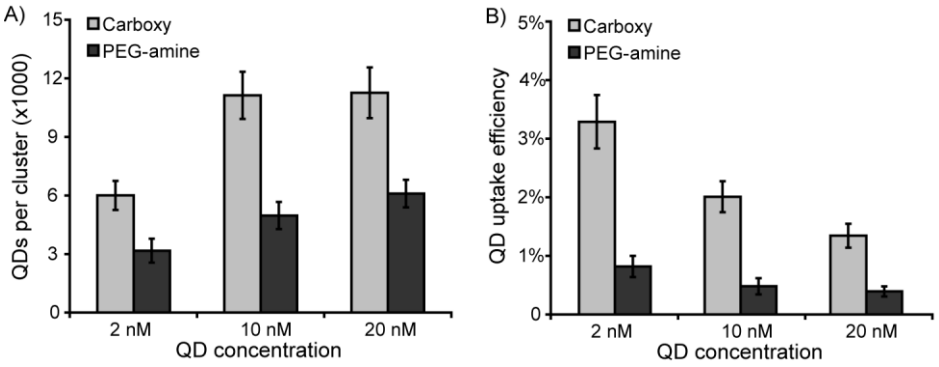

Supplementary Figure S2. Cellular QDot levels in C17.2 cells. **A)** The number of QDots per cluster and **B)** cellular uptake efficiency of QDots for C17.2 cells in function of the QDot concentration for both carboxy (light grey)- and PEG-amine QDots (dark grey) after 24 h exposure. Data are shown as mean ± SEM (n = 4) and indicate that at high intracellular QDot levels, the number of QDots per cluster appears to be limited, where further increases in total cellular QDot levels are then due to a higher number of QDot clusters. Furthermore, at higher QDot concentrations, a higher total number of QDots is observed, but the uptake efficiency decreases, indicative of a saturable uptake mechanism.

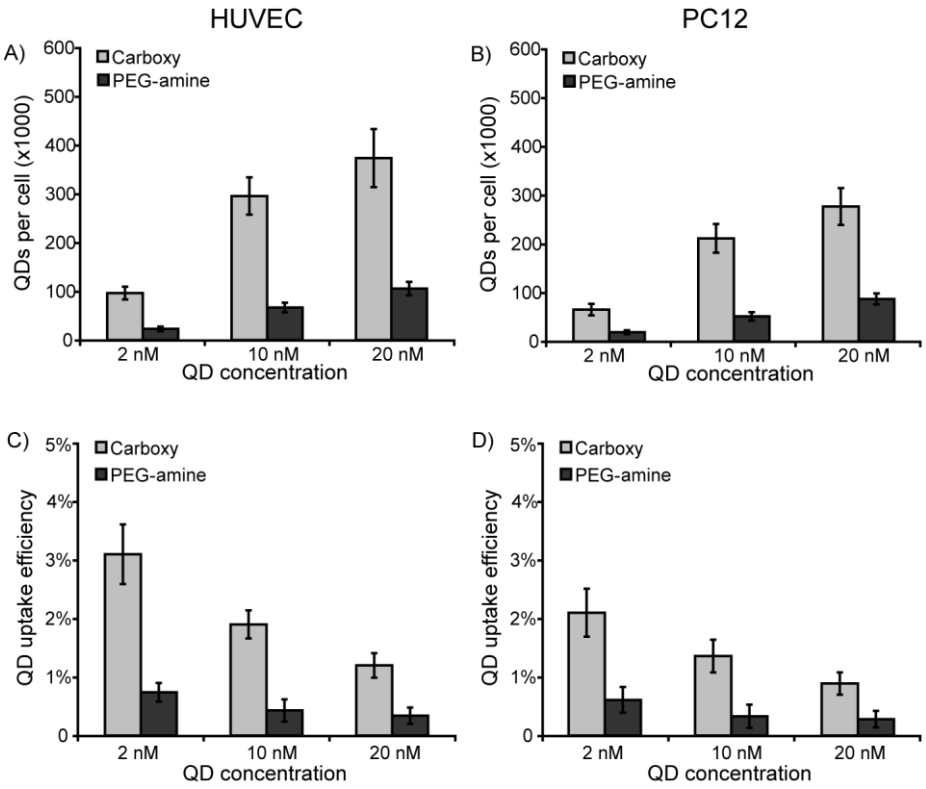

Supplementary Figure S3. Cellular QDot levels in HUVECs and PC12 cells as determined by measuring fluorescence intensity levels. **A,B)** The number of total QDots per cell and **C,D)**

cellular uptake efficiency of QDots in function of the QDot concentration for both carboxy (light grey)- and PEG-amine QDots (dark grey) after 24 h exposure. **A,C)** Data for HUVEC cells, **B,D)** for PC12 cells. Data are shown as mean ± SEM (n = 4) and indicate the similarity in cellular QDot levels for C17.2 and HUVEC cells and PC12 cells. The latter cell type has a slightly lower uptake efficiency which is likely due to its small size and limited cell surface area, which decreases the chance of interaction of the QDots with the cell membranes, which is a prerequisite for cellular uptake.

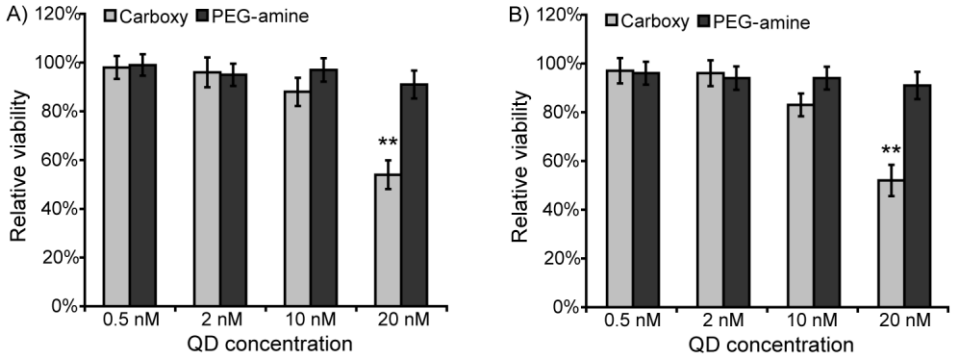

Supplementary Figure S4. Effects of QDots on HUVEC and PC12 cell viability. **A,B)** Cellular viability as a function of QDot concentration for both carboxy- and PEG-amine QDots after 24 h incubation for **A)** HUVEC cells and **B)** PC12 cells. Data are represented as mean ± SEM (n = 8) and expressed as relative to untreated control cells, showing large similarities in terms of the acute toxicity of the QDots on all three cell types, where acute cytotoxic effects are observed for carboxy-QDots at 20 nM. When appropriate, the degree of significance is indicated when compared to untreated control cells (**: $p < 0.01$).

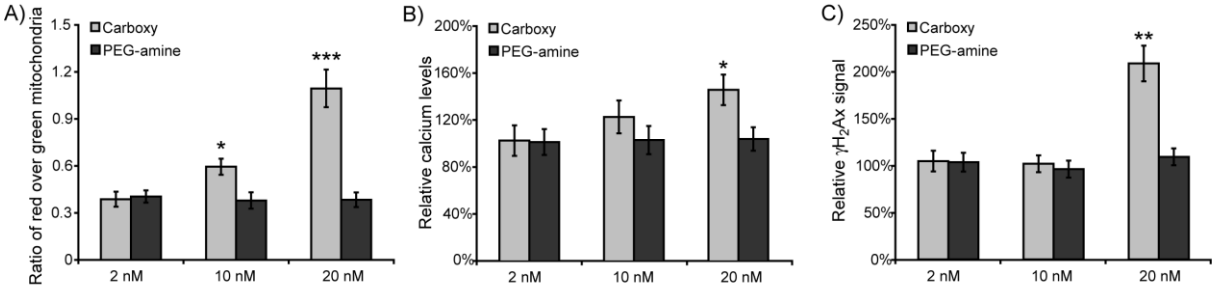

Supplementary Figure S5. Secondary QDot-induced ROS effects in C17.2 cells. **A)** Quantitative levels of JC-10 for C17.2 cells exposed for 24 h to different concentrations of carboxy (light gray)- or PEG-amine QDots (dark grey). Upon mitochondrial injury, the green fluorescent JC-10 dye will form red clusters inside the damaged mitochondria, so the ratio of

red over green mitochondria indicates the integrity of the mitochondria. **B)** Relative levels of cellular calcium as determined by the Fluo-4 assay for C17.2 cells exposed for 24 h to different concentrations of carboxy (light gray)- or PEG-amine QDots (dark grey). **C)** Relative levels of γ-H_2Ax, which is phosphorylated upon DNA cleavage and thus acts as a marker for DNA damage, for C17.2 cells exposed for 24 h to different concentrations of carboxy (light gray)- or PEG-amine QDots (dark grey). Data are expressed as mean ± SEM (*n* = 3). When appropriate, the degree of significance is indicated (*: $p < 0.05$; **: $p < 0.01$; ***: $p < 0.001$). These data indicate the occurrence of several side-effects commonly associated with high cellular ROS levels for cells containing the highest levels of QDots (i.e. the 20 nM carboxy-QDots exposure).

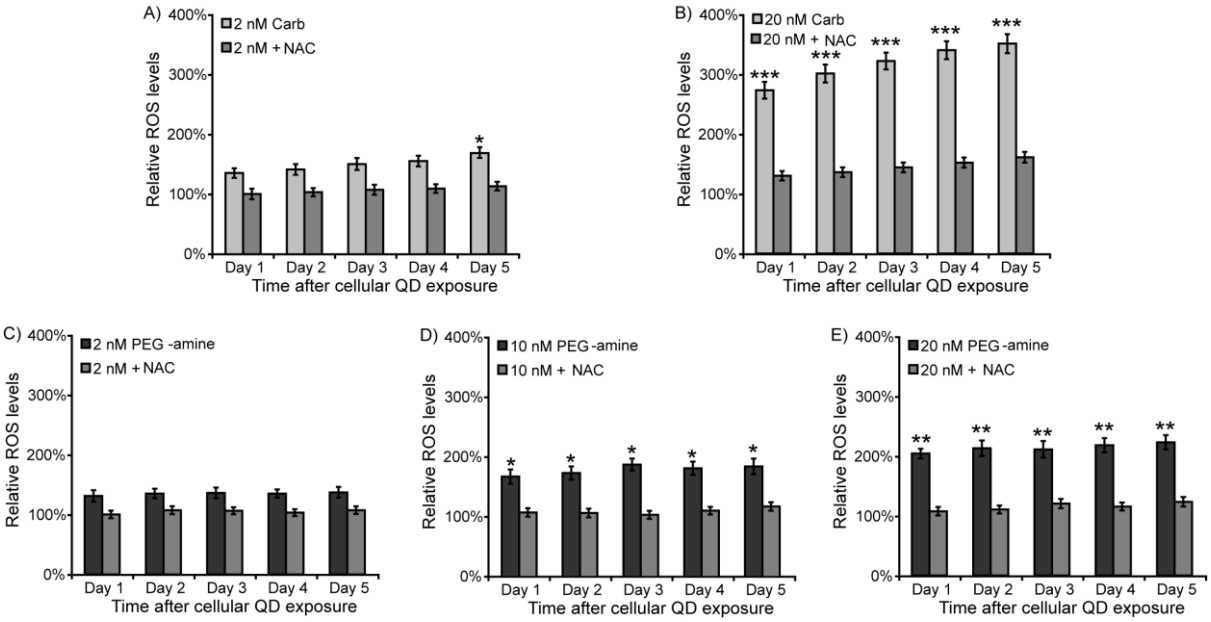

Supplementary Figure S6. Levels of ROS in non-proliferating C17.2 cells. **A-E)** Levels of ROS in non-proliferating C17.2 cells exposed to **A)** 2 nM or **B)** 20 nM carboxy-QDots or **C)** 2 nM, **D)** 10 nM or **E)** 20 nM PEG-amine QDots for 24 h and subsequently analyzed for ROS after 1, 2, 3, 4 or 5 days of additional culture showing a clear increase in cellular ROS levels. Exposure of C17.2 cells in the presence of 5 mM NAC significantly reduces ROS. Data are expressed as mean ± SEM (*n* = 8) against 60 µM Apigenin-treated control cells. The degree of statistical significance of treated samples versus control samples is indicated when appropriate (*: $p < 0.05$; **: $p < 0.01$; ***: $p < 0.001$).

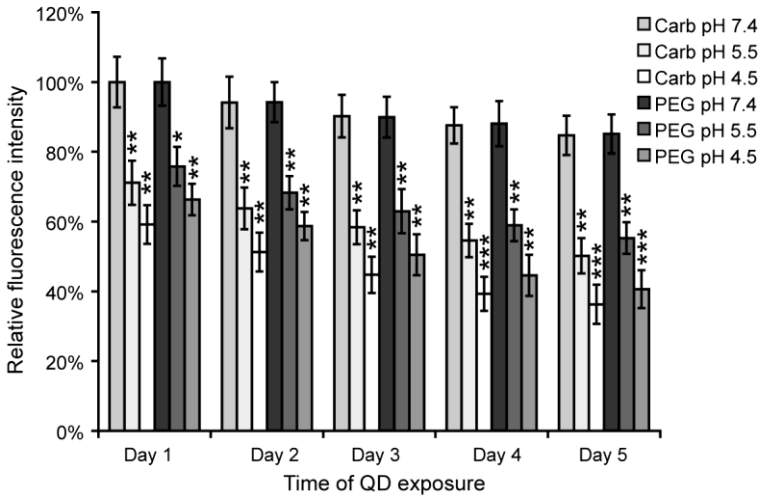

Supplementary Figure S7. Effect of pH on QDot fluorescence intensity. Relative fluorescence intensity levels of 5 nM suspensions of either carboxy- or PEG-amine QDots at various pH values (7.4, 5.5, 4.5) as a function of time showing a clear time-dependent and pH-mediated loss of fluorescence of either type of QDot. Data are expressed as mean ± SEM (n = 3) and the degree of statistical significance of treated samples versus control samples is indicated when appropriate (**: $p < 0.01$; ***: $p < 0.001$). As these pH values correspond to the values typically found in the cell cytoplasm (7.4), early to late endosomes (5.5) and lysosomes (4.5), the rapid pH-mediated loss of fluorescence likely also occurs in cells, where the gradual loss of fluorescence can be attributed to acid etching of the QDot surface as shown by the release of Cd^{2+}.

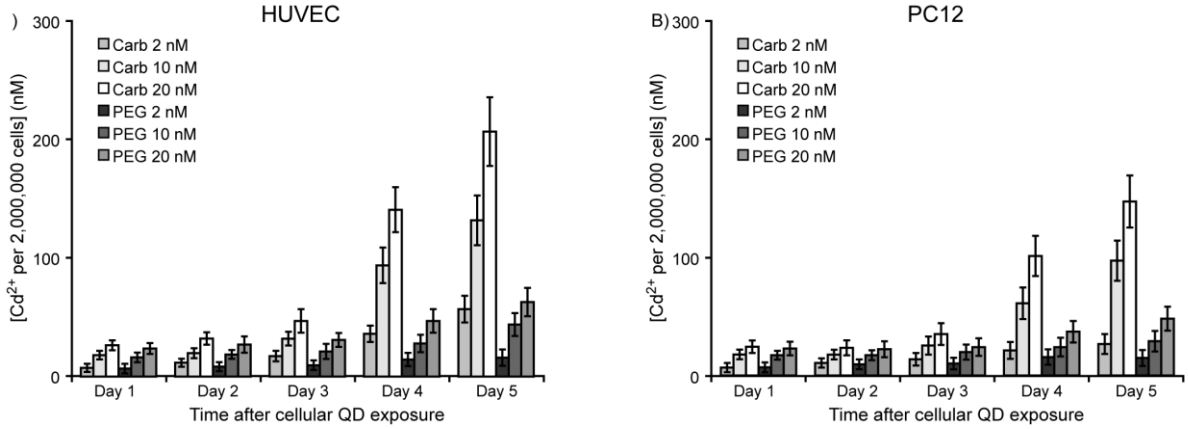

Supplementary Figure S8. Effect of intracellular QDot degradation on Cd^{2+} generation in HUVEC and PC12 cells. **A,B)** Levels of free Cd^{2+} in **A)** HUVEC cells and **B)** PC12 cells exposed to either carboxy- or PEG-amine QDots for 24 h and subsequently kept in non-proliferating state after which the cellular Cd^{2+} levels are measured after 1, 2, 3, 4 and 5 days. The data show the same trend as observed for C17.2 cells, where a clear time-dependent increase in cellular Cd^{2+} levels is noticed, being more outspoken for the carboxy-QDots,

which is in line with their much higher cellular uptake efficiency. Data are expressed as mean ± SEM (n = 3).

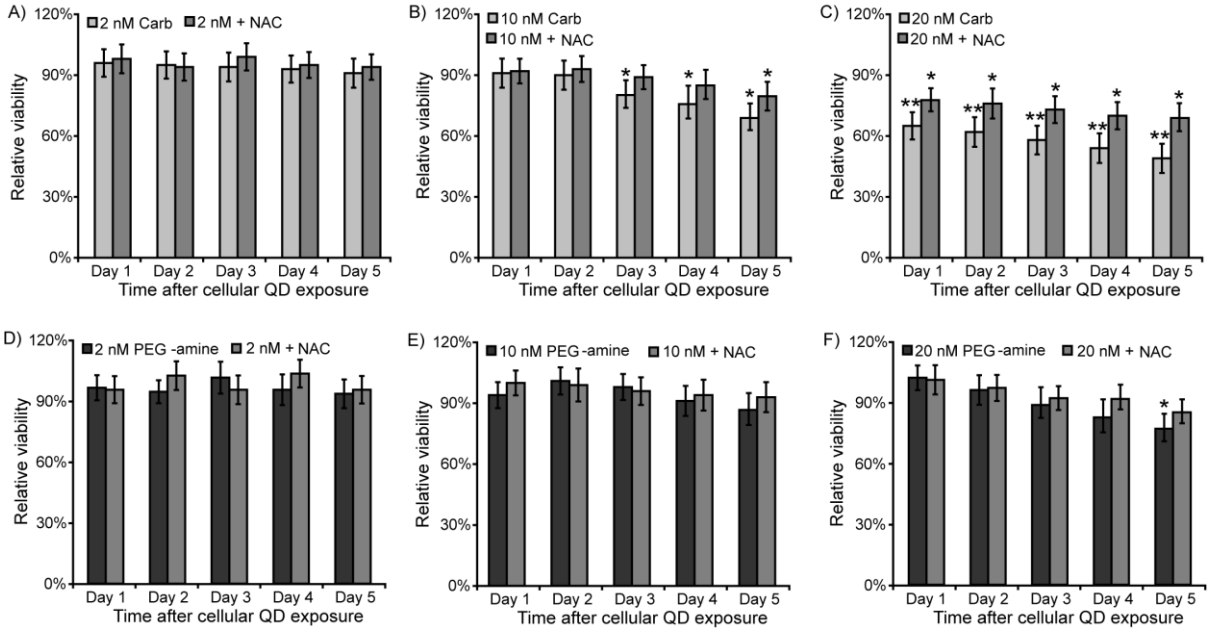

Supplementary Figure S9. Effect of QDots on the viability of proliferation-restricted C17.2 cells. **A-F)** Viability of C17.2 cells as a function of QDot concentration following 24 h incubation with either **A)** 2nM, **B)** 10 nM or **C)** 20 nM carboxy- and **D)** 2 nM, **E)** 10 nM or **F)** 20 nM PEG-amine QDots after 24 h incubation. Data are expressed as a function of time for cells kept in non-proliferative state after QDot exposure. Data are represented as mean ± SEM (n = 8) and expressed as relative to untreated non-proliferative (60 µM Apigenin-treated) control cells, showing a clear time-dependent reduction in cell viability for the highest concentrations of both carboxy- and PEG-amine QDots. When appropriate, the degree of significance is indicated when compared to untreated control cells (*: $p < 0.05$; **: $p < 0.01$).

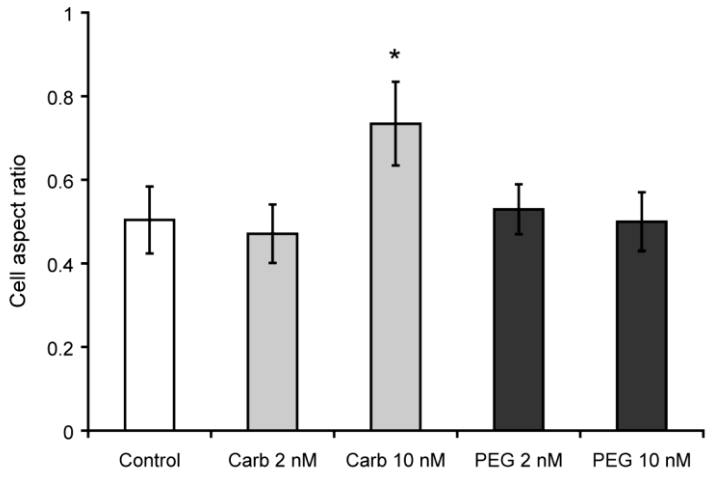

Supplementary Figure S10. Effect of QDots on the polarity of HUVEC cells. Cellular aspect ratio (ratio of cellular width over cellular length) for HUVEC cells either not exposed to any particles or exposed to 2 nM or 10 nM of either carboxy- or PEG-amine QDots for 24 h and subsequently stained for α-tubulin after 3 additional days of culture. For the HUVEC cells, which typically show a rather lengthened morphology, a higher cell aspect ratio, as observed for cells exposed to 10 nM carboxy-QDots, indicates rounding up of the cell and loss of cell spreading. Data are expressed as mean ± SD (n = 20) and when appropriate, the degree of significance is indicated when compared to untreated control cells (*: $p < 0.05$). Similar results with respect to cell aspect ratio and cell spreading were also observed for C17.2 cells (data not shown).

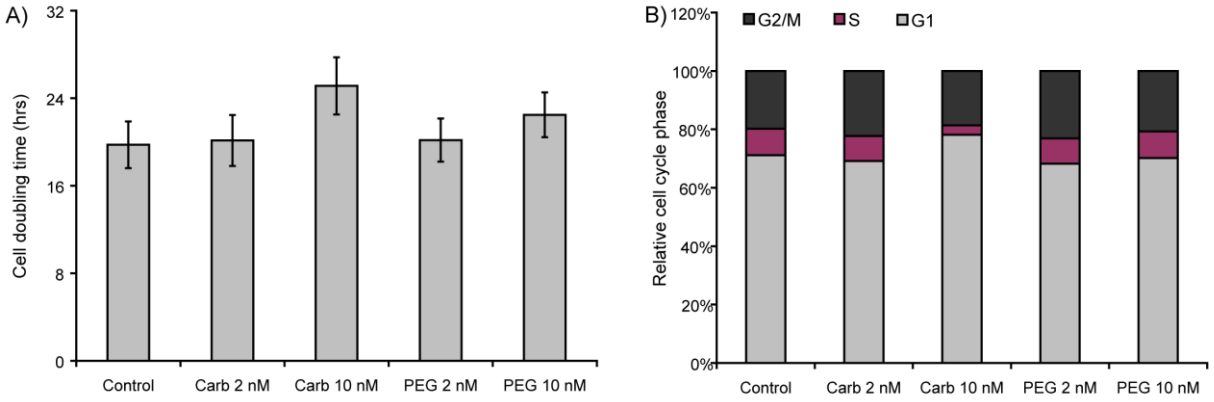

Supplementary Figure S11. Effect of QDots on cell cycle progression. **A)** Cell doubling time of C17.2 cells either not exposed to any particles or exposed to 2 nM or 10 nM of either carboxy- or PEG-amine QDots for 24 h. Data are expressed as mean ± SEM (n = 4), showing a slight but not significant increase in cell doubling time for C17.2 cells exposed to 10 nM carboxy-QDots. **B)** The respective C17.2 cell cycle statuses of control cells or cells incubated with QDots for 24 h assessed at 3 days after QDot incubation by flow cytometry. The relative amount of cells in G1 phase is indicated in light grey, S phase in purple and G2/M phases in

dark grey. The data show a clear, but non-significant reduction in cell cycle progression for C17.2 cells exposed to 10 nM carboxy-QDots. The correlation of the loss of cell spreading and the slight decreases in cell proliferation at higher intracellular nanoparticle concentrations is in line with previous reports on iron oxide particles, where cytoskeletal disturbances (due to steric hindrance by the large number of nanoparticle-loaded endosomes or by ROS generation) affected cytoskeletal-mediated signaling, resulting e.g. in reduced cell proliferation.

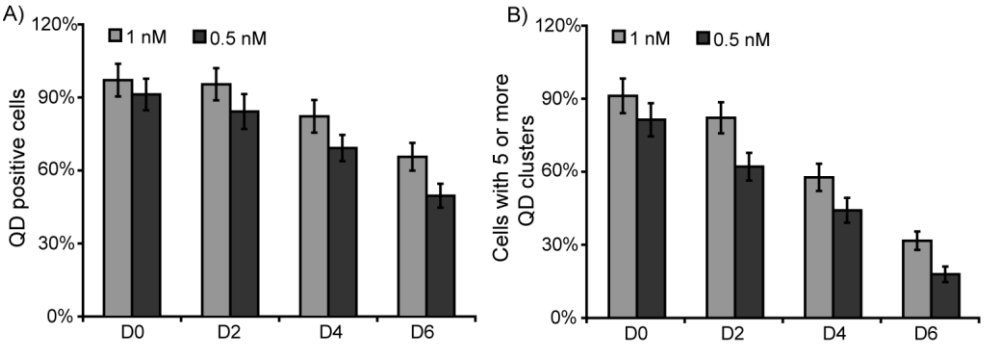

Supplementary Figure S12. Effect of cell division on cellular transfer of carboxy-QDots. The percentage of **A)** QDot-positive C17.2 cells or **B)** C17.2 cells containing 5 or more QDot clusters for cells incubated with 1 nM or 0.5 nM carboxy-QDots for 24 h after 0, 2, 4 and 6 average cell doubling times as evaluated by microscopy analysis. The data are expressed as mean $\pm$ SEM (n = 3).

Supplementary Materials and Methods.

Endosomal localization of QDots. To assess the possible endosomal localization of the QDots, C17.2 cells were seeded in collagen-coated 35 mm diameter glass bottom MatTek dishes (MatTek Corporation, Ashland, MA, USA) at $4*10^4$ cells/dish in 1.5 ml of full culture medium. Cells were allowed to settle overnight prior to being incubated with the lipophilic membrane tracer dye 3,3′-dioctadecyloxacarbocyanine perchlorate (DiO; Molecular Probes, Invitrogen, Belgium) for 30 min at 2.5 µg/ml. Next, a mixture of either type of QDot at 15 nM and the lipophilic dye DiO (2.5 µg/ml) in full cell medium was prepared and added to the cells for 30 min at 37°C at a humidified atmosphere. Subsequently, the media were removed, cells washed three times with PBS and fixated with 4% paraformaldehyde (PFA) for 15 min at ambient temperature prior to visualization using a Nikon Cs1 confocal laser scanning microscope (Nikon Belux, Brussels, Belgium).

For a 3D overview of intracellular QDot distribution (Supporting Figure S1), C17.2 cells were treated in a similar manner, where prior to fixation, cells were exposed to 4'-6-Diamidino-2-phenylindole (DAPI) nuclear counterstain for 10 min at ambient temperature, followed by three washing steps with PBS and confocal visualization. For every cell, a series of images along the z-axis were obtained with 0.5 µm interslice distance, starting from the top of the cell towards the bottom.

QDot bleaching experiments. The photostability of cell-internalized QDots was tested using HUVEC cells, which were seeded in collagen-coated 35 mm diameter glass bottom MatTek dishes at $4*10^4$ cells/dish in 1.5 ml of full culture medium. Cells were allowed to settle overnight after which the media were aspirated and fresh media containing either carboxy- or PEG-amine QDots at 2 nM was added and cells were incubated with the particles for 24 h at 37°C and 5% CO_2 in a humidified atmosphere. Media were then aspirated, cells washed three times with PBS, fixated with 4% PFA, permeabilised with 0.1% Triton X-100 for 10 min and then blocked with 10% goat serum-containing PBS for 30 min. Then, cells were incubated with primary murine antibody in blocking buffer against α-tubulin (1 µg/ml; Abcam, Cambridge, UK) for 2 h at ambient temperature. Cells were washed three times with blocking buffer after which they were incubated with secondary AF488-conjugated goat anti-murine IgG antibody (1/250 dilution; Molecular Probes, Invitrogen, Belgium) for 1 h at ambient temperature. Cells were then washed three times with PBS prior to viewing by confocal microscopy. To assess the extent of photobleaching, the selected cells were exposed to the

304 and 488 nm lasers of the confocal unit at 15% power and images were acquired at every sweep of the lasers. The images in Supplementary Figure S13 are shown for randomly selected time points following initial exposure. For a quantitative determination of fluorescence intensities, the intensity of both the AF488 and 565-QDots were measured for 10 cells per condition, each from a different specimen.

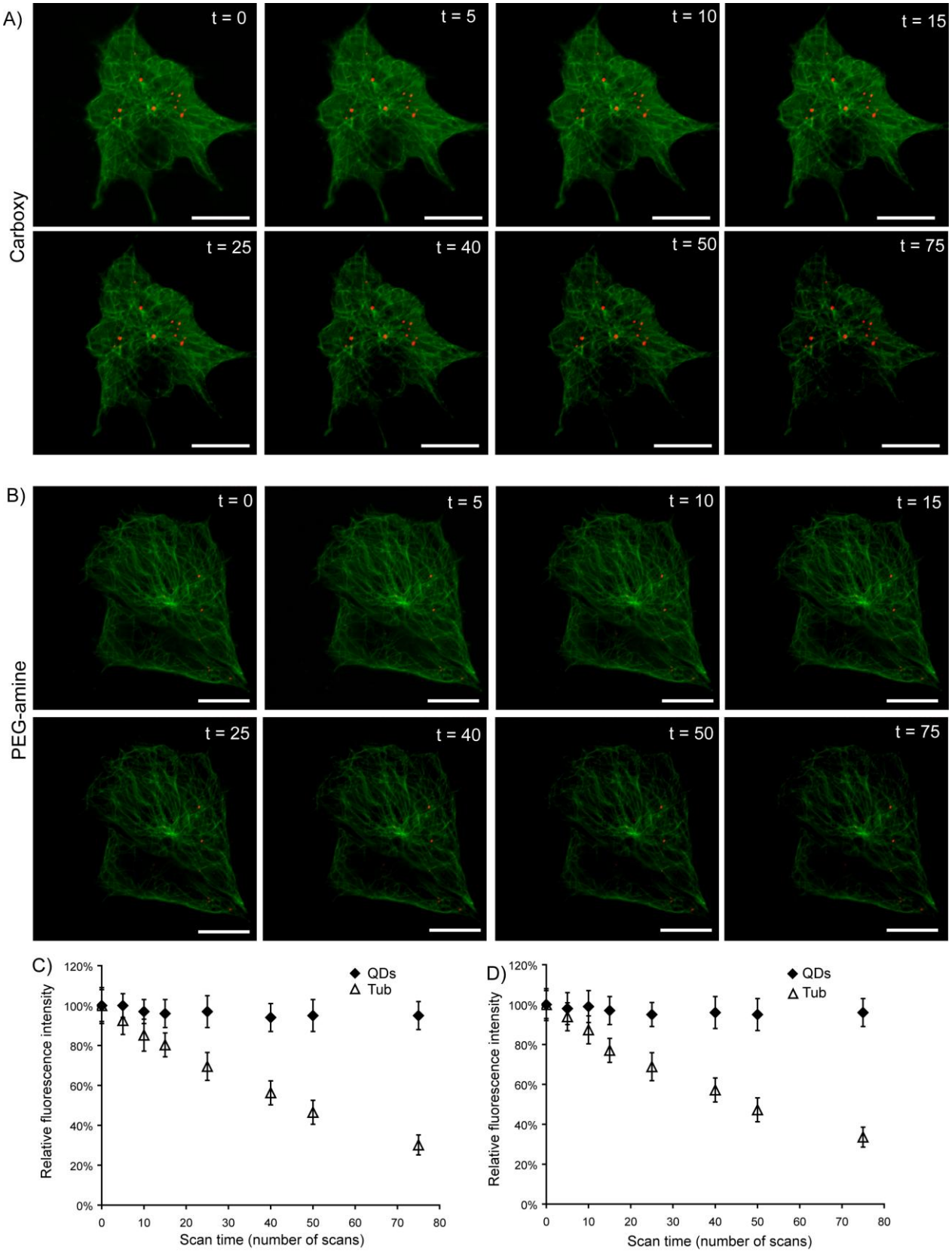

Supplementary Figure S13. Photostability of QDots. **A,B)** Representative confocal images of HUVEC cells incubated for 24 h with 2 nM **(A)** carboxy-QDots or **(B)** PEG-amine QDots. The images show the QDots (red) and α-tubulin cytoskeleton (green by immunostaining). The

number in the top right corner indicates the number of scans that the image was exposed to upon acquisition, showing a clear bleaching for the AF488-stained α-tubulin cytoskeleton whereas the QDots do not appear to bleach. **C,D)** The relative fluorescence intensities of HUVEC cells exposed to 2 nM **(C)** carboxy-QDots or **D)** PEG-amine QDots for 24 h and subsequently stained for α-tubulin. The data are expressed as mean ± SEM (n = 10), showing a clear loss of fluorescence intensity for AF488 upon light exposure whereas no differences in fluorescence intensities can be observed for the QDots.

Quantitative determination of cellular QDot levels. Determination of the number of QDots per cell occurred through various protocols. In literature, cellular QDot levels are mostly defined as the number of QDot clusters per cell, as assessed by microscopy analysis. Here, the number of QDot clusters were counted for a total of 100 cells per condition using ImageJ (NIH, USA). A total of 4 independent repeats were performed after which the number of clusters per well and the respective standard error to the mean were calculated as shown in Figure 1c.

Assessing the number of QDots per cell is highly interesting in terms of better understanding the toxicological aspects involved. However, in most studies, the cellular amount of QDots is not determined, likely due to a lack of standard protocols. Here, we determined the cellular amount of QDots by means of two different approaches. To start, cells (either C17.2, PC12 or HUVEC cells) were seeded in 75 cm² cell culture flasks at $3*10^6$ cells/flask and allowed to settle overnight. Then, medium was aspirated and replaced by fresh medium containing either carboxy- or PEG-amine QDots at 2, 10 or 20 nM (total volume: 10 ml per flask). Cells were then allowed to incubate with the particles for 24 h at 37°C. The medium was then aspirated, cells washed 3 times with PBS and cells were lifted by trypsin. Cells were then centrifuged at 0.4 rcf after which the cell pellets were collected and the supernatants removed. The next steps differed depending on the type of assay performed. For the first approach, the cell pellets were resuspended in 100 µl of HCl/HNO_3 (3/1) and left at 37°C for 48 h to allow acid-induced degradation of the cells and the QDots, resulting in free Cd^{2+}. Next, 25 µl of this suspension was collected and diluted to 100 µl using a 0.2 M phosphate buffer, pH 8.4. From this dilution, 10 µl of every sample was taken and transferred to different wells of a 96-well plate after which 200 µl/well of the Measure-iT kit (Molecular Probes, Invitrogen, Merelbeke, Belgium) was added and Cd^{2+} concentrations were measured according to the manufacturer's instructions (λ_{ex}: 490 nm; λ_{em}: 520 nm) using a Wallac Envision plate reader instrument (Perkin Elmer, Zaventem, Belgium). The Cd^{2+} concentration was then recalculated to QDot

concentrations using a dilution series of the QDot stock solutions treated under identical conditions (See Supplementary Figure S14).

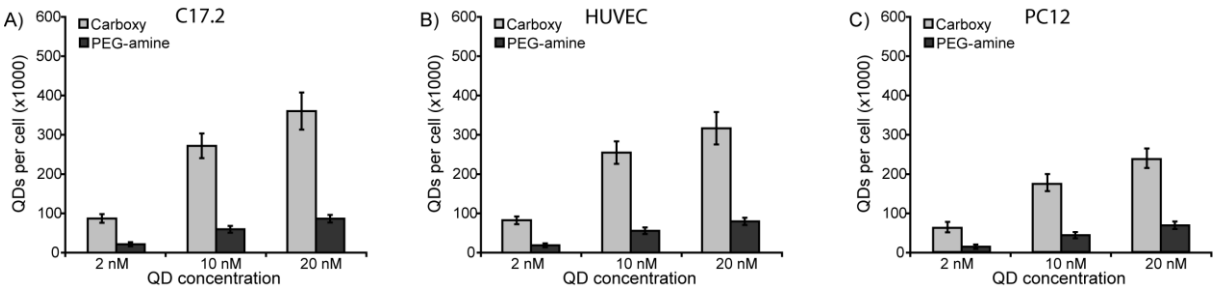

Supplementary Figure S14. Cellular QDot levels in C17.2 cells, HUVECs and PC12 cells as determined by measuring total Cd^{2+} levels. **A-C)** The number of total QDots per cell for **A)** C17.2 cells, **B)** HUVEC cells and **C)** PC12 cells as a function of QDot concentration for both carboxy (light grey)- and PEG-amine QDots (dark grey) after 24 h exposure as determined by acid hydrolysis of QDot-containing cell pellets and measured by the Measure-iT kit, which determines the concentration of free Cd^{2+} ions. Data are expressed as mean $\pm$ SEM (n = 3) and show a high similarity in the number of QDots calculated using by fluorescence analysis of osmolytically destroyed cells as done for the previous studies (see Figure 1 and Supplementary Figure S4).

For the second method, the cell pellets were incubated in 200 µl of a 0.2 M phosphate buffer, pH 8.4 for 48 h in order to lyse the cells and obtain clear QDot suspensions. From these suspensions, 150 µl per sample was transferred to different wells of a black 96-well plate after which the fluorescence intensity levels were determined using a Wallac Envision plate reader instrument (λ_{ex}: 305 nm; λ_{em}: 560 nm). The fluorescence intensity values were then transformed to QDot concentrations using a dilution series of the QDot stock solutions treated under identical conditions. As the fluorescence intensity of the QDots is highly sensitive to the surrounding pH, cells were lysed deliberately with a stable buffer with slightly basic pH value to avoid any artifacts in fluorescence intensity levels due to different subcellular localizations of the different QDots. Furthermore, as nearly all detergents used resulted in interferences in the fluorescence profiles, a detergent-free cell lysis approach was selected, using a buffer of low osmolarity. For these assays, a total of 4 independent experiments were carried out. The number of QDots per clusters could simply be calculated by dividing the average number of QDots per cell by the average number of clusters per cell. The cellular uptake efficiency could be calculated by dividing the cellular amount of QDots over the number of QDots to which the cells were initially exposed.

Determination of cell viability upon acute QDot exposure. Quantitative cell viability data were generated using an MTT (Sigma-Aldrich, Bornem, Belgium) and a Lactate Dehydrogenase (LDH) assay (Promega, Madison, USA). For the MTT assay, C17.2, HUVEC or PC12 cells were seeded at $5*10^4$ cells/well in 96-well plates (200 µl/well total volume) and allowed to settle overnight. Next, cells were incubated with the QDots at 0, 0.5, 2, 10 or 20 nM for 24 h, after which the MTT assay was performed according to the manufacturer's protocol (25 µl of a 5 mg/ml solution of MTT salt added to every well and incubated for 4 h). Untreated cells were assayed as a control reference and untreated cells exposed to 0.1% Triton X-100 for 15 min were used as negative controls. For the LDH assay, C17.2, HUVEC or PC12 cells were seeded at $2*10^4$ cells/well in 96-well plates (150 µl/well total volume) and allowed to settle overnight. Next, cells were incubated with the QDots at 0, 0.5, 2, 10 or 20 nM for 24 h, after which the LDH assay was performed according to the manufacturer's protocol. Untreated cells were assayed as a control reference and untreated cells exposed to 0.1% Triton X-100 for 15 min were used as negative controls. For every condition, 8 independent measurements were performed.

As nanomaterials are rumored to lead to possible interferences with common cell viability assays, additional controls were taken into account. First, the values for both the MTT and LDH assay were compared and were found to never diverge more than 12%. Second, QDot-incubated cells were also treated with 0.1% Triton X-100 for 15 min and were found to lead to similar toxicity levels as the negative controls, indicating that the presence of the QDots did not have any effect on the release profile of LDH. Third, medium which contained the QDots in the absence of any cells was analyzed, showing no signal for the presence of LDH, indicating that the particles do not interfere with the assay readout itself at the concentrations used in the present study. Fourth, cells were also treated normally and incubated with the QDots after which an LDH or MTT assay was performed similar to the normal protocol but with omission of the LDH substrate or MTT salt, which resulted in no signal obtained. As the toxicity values for both types of assays were very similar, only the data for the MTT assay are shown.

Determination of reactive oxygen species. To measure induced ROS levels, C17.2 cells were seeded at $5*10^4$ cells/well in non-transparent 96 well plates (Greiner Bio One, Wemmel, Belgium) and allowed to settle overnight after which the cells were incubated with the QDots at 0, 2, 10 or 20 nM for 24 h. Then, the cells were washed 3 times with PBS and incubated

with 10 µM 5-(and-6)-chloromethyl-2',7'-dichlorodihydrofluorescein diacetate, acetyl ester (CM-H_2DCFDA; Molecular Probes, Invitrogen, Merelbeke, Belgium) for 45 min followed by an additional incubation for 30 min in full culture medium. Then, the cells were washed twice with PBS and the fluorescence signal was measured using a Wallac Envision plate reader instrument with an excitation filter of 480 nm and an emission filter of 540 nm. For a positive control, cells were incubated with 1% H_2O_2 for 2 h prior to incubation with CM-H_2DCFDA. Data are expressed relative to untreated control cells (= 100%) as mean $\pm$ SEM (n = 8). Additional controls treated similarly but without addition of CM-H_2DCFDA or the addition of QDots and CM-H_2DCFDA in the absence of cells did not give any significant signals, verifying the induction of ROS in the cells due to the QDots and lack of QDot interference with the ROS assay.

To measure ROS levels at different time points, C17.2 cells were seeded at $5*10^4$ cells/well in non-transparent 96 well plates and labeled with the QDots as described above. For C17.2 cells, 60 µM Apigenin was also added. Then, media were removed and cells were further cultured under non-proliferative conditions, after which ROS levels were determined after 1, 2, 3, 4 and 5 days of further culture. Data are expressed relative to proliferation-inhibited control cells which were not exposed to any QDots (= 100%) as mean $\pm$ SEM (n = 8). Of interest, under these conditions, no significant increase in ROS levels were noted for proliferation-inhibited cells compared to actively proliferating cells. To further verify whether the observed inductions of ROS were caused by intracellular QDots, cells were also exposed to 5 mM N-acetyl-cysteine (NAC; Sigma-Aldrich, Bornem, Belgium), a potent free radical scavenger, for the duration of the experiment. NAC was found to significantly reduce ROS levels in all conditions to near control levels, supporting that ROS induction occurred by intracellular QDots (Figure 2c, Supplementary Figure S9).

Determination of cell viability in proliferation-restricted cells. Quantitative cell viability data were generated by an LDH assay (Molecular Probes, Invitrogen, Merelbeke, Belgium). To this end, C17.2 cells were seeded at $2*10^4$ in non-transparent 96-well plates and allowed to settle overnight. Next, cells were incubated with the QDots at 0, 2, 10 or 20 nM for 24 h in the presence of 60 µM Apigenin, after which media were removed and cells were kept in culture in 60 µM Apigenin-containing media. After 1, 2, 3, 4 and 5 days of further culture, the LDH assay was performed as described above. Untreated cells were assayed as a control reference and untreated cells exposed to 0.1% Triton X-100 for 15 min were used as negative controls.

Data are expressed as mean ± SEM (n = 8). Under these conditions, proliferation-restricted cells were not found to lead to toxic effects compared to proliferating cells, but the impeded proliferation did reduce cell metabolism, which made the MTT assay not applicable under these conditions.

To evaluate the contribution of ROS levels to QDot-induced cytotoxicity, cell viability was also measured for cells co-exposed to 5 mM NAC for the duration of the experiment. Supporting Figure S12 shows that NAC partially reduced the cytotoxic effects of the QDots, but could not completely overcome QDot-induced cytotoxicity at the highest levels of carboxy-QDots, suggesting other mechanisms responsible for QDot-induced toxicity at higher intracellular concentrations.

Determination of pH effects on QDot stability. To assess possible endo- and lysosomal degradation of the QDots, an *in vitro* model system was used as described previously [1]. For these experiments, three different buffer systems were used which consist of PBS, supplemented with 40 mM sodium citrate to which an equal amount of 20% serum-containing, high glucose cell culture medium (DMEM) was added. Next, the buffer was divided in 3 parts and the pH of the respective buffer systems was adjusted to 7.4, 5.5 or 4.5 using HCl (2 N), equaling the pH of the cell cytoplasm, endosomes and lysosomes, respectively. As such, these buffer systems contain 10% serum (the physiologically relevant concentration as used for most cell culture conditions). These buffer systems were then filter sterilized using a 0.20 μm filter (Sartorius Minisart, Vivascience, Hannover, Germany) and were further used in the experiments described below.

To evaluate the effect of the pH on the fluorescence intensity of QDots, both types of QDot stock suspensions were diluted up to 2 ml using the three buffer systems, reaching a final concentration of 5 nM of QDots. These suspensions were then transferred to 10 wells per sample of a black 96 well plate (200 μl/well) and placed at 37°C and 5% CO_2 in a humidified atmosphere to better simulate the intracellular environment. Fluorescence intensity levels were determined using a Wallac Envision plate reader instrument (λ_{ex}: 305 nm; λ_{em}: 560 nm) after 1, 2, 3, 4 and 5 days of further incubation. Data are expressed as mean ± SEM of three independent experiments and given relative to the values obtained for 5 nM QDots diluted in 10% serum-containing PBS at the initial time point.

The generation of free Cd^{2+} ions as a result of acid etching of the QDots under these conditions were measured by diluting the QDot stock suspensions up to 1 ml in the three buffer systems, reaching a final concentration of 10 nM of QDots. These suspensions were then placed at 37°C and 5% CO_2 in a humidified atmosphere for the duration of the experiment. After 1, 2, 3, 4 and 5 days of incubation, 10 µl per sample was collected and transferred to different wells of a 96-well plate after which 200 µl/well of the Measure-iT kit was added and Cd^{2+} concentrations were measured according to the manufacturer's instructions (λ_{ex}: 490 nm; λ_{em}: 520 nm) using a Wallac Envision plate reader instrument. The Cd^{2+} concentrations were determined using the Cd^{2+} calibration curve which is part of the kit. Data are expressed as mean ± SEM for three independent experiments.

Determination of intracellular QDot degradation. C17.2, PC12 or HUVEC cells were seeded in 75 cm² cell culture flasks at a density of $5*10^6$ cells/flask and allowed to settle overnight. Then, the cells were given fresh medium containing 0, 2, 10 or 20 nM of QDots and allowed to incubate for 24 h. For C17.2 and PC12 cells, their medium was supplemented with 60 µM Apigenin. Next, the media were aspirated, cells washed twice with PBS and given fresh media optimized for non-proliferating cultures as described above after which the cells were kept in culture for the duration of the experiment. After 1, 2, 3, 4 and 5 days of further culture under proliferation-restricted conditions, cells from the various flasks were lifted and centrifuged at 0.4 rcf. The cells were redispersed in PBS and counted using a Bürker chamber. Then, $2*10^6$ cells were taken, which were centrifuged again after which 50 µl of DMSO was added to every pellet to lyse all cells. A 10 µl aliquot was collected from every sample and transferred to wells of a 96-well plate after which 200 µl/well of the Measure-iT kit was added and Cd^{2+} concentrations were measured according to the manufacturer's instructions (λ_{ex}: 490 nm; λ_{em}: 520 nm) using a Wallac Envision plate reader instrument. The Cd^{2+} concentrations were determined using the Cd^{2+} calibration curve which is part of the kit. Please note that as this is an end-point assay, the samples measured after 1, 2, 3, 4, and 5 days were all obtained from different flasks. Data are expressed as mean ± SEM for three independent experiments.

Determination of HUVEC cell morphology. For analysis of cell morphology, HUVEC cells were seeded in 25 cm² cell culture flasks at $1*10^6$ cells/flask and allowed to settle overnight. Then, media were replaced with fresh media containing 0, 2 or 10 nM of either type of QDots and cells were incubated with the QDots for 24 h. Media were then aspirated, cells washed

twice with PBS and fresh medium was given after which the cells were kept in culture for 1 more day. Then, cells were lifted and seeded in collagen-coated 35 mm diameter glass bottom MatTek dishes (MatTek Corporation, Ashland, MA, USA) at $2*10^4$ cells/dish in 1.5 ml of full culture medium. After seeding, cells were kept in culture for another 48 h. Next, cells were washed three times with PBS, fixed for 20 min in 2% PFA, permeabilized with 1% Triton X-100 for 15 min and blocked using 10% goat serum (Gibco, Invitrogen, Belgium)-containing PBS for 30 min. Then, cells were incubated with primary murine antibody in blocking buffer against α-tubulin (1 µg/ml; Abcam, Cambridge, UK) for 2 h at ambient temperature. Cells were washed three times with blocking buffer after which they were incubated with secondary AF488-conjugated goat anti-murine IgG antibody (1/250 dilution; Molecular Probes, Invitrogen, Belgium) for 1 h at ambient temperature. Cells were then washed three times with PBS and maintained in 1.5 ml PBS at 4°C prior to viewing by a Nikon Cs1 confocal laser scanning microscope.

For calculations of cell areas, fluorescence images were taken at a 20x magnification and areas were calculated using ImageJ software (NIH, USA) for at least 150 cells/sample. Cell aspect ratios were determined by drawing a straight line on the high magnification (60x) confocal images, along the cell axis and another one perpendicular to it, spanning the maximum length and width of the cell, respectively. The length of the first line was divided by the length of the second one to determine the cell aspect ratios. A total of 40 images per condition were analyzed. For both experiments, images were collected from 4 independently prepared sample per condition.

Determination of PC12 functionality. To assess the ability of PC12 cells to produce neurites, PC12 cells were seeded in collagen-coated 35 mm diameter glass bottom MatTek dishes (MatTek Corporation, Ashland, MA, USA) at $2*10^4$ cells/dish in 1.5 ml of full culture medium. Cells were allowed to settle overnight prior to being incubated with the QDots for 24 h at 0, 1, 2 or 5 nM for carboxy-QDots and 5 or 10 nM for PEG-amine QDots. After incubation, cells were washed twice with PBS and fresh medium was given and cells were kept in culture for another 12 h. Then, cells were washed three times with PBS after which cells were given nerve growth factor (NGF) induction medium, consisting of high glucose DMEM, supplemented with 1% fetal calf serum, 5% horse serum, 1 mM sodium pyruvate, 2 mM L-Glutamine, 1% penicillin/streptomycin and 100 ng/ml NGF (Sigma-Aldrich, Bornem, Belgium). Cells were kept in this medium for 72 h where after every 24 h, half the medium

was replaced by fresh induction medium. Samples were then fixed, permeabilized and stained for α-tubulin as described above, after which the samples were viewed using a Nikon Cs1 confocal laser scanning microscope. Using images acquired at a low magnification (20x) processing occurred using ImageJ, where the number and length of neurites - defined as having twice the length of the cell body - were calculated using an ImageJ plug-in called NeuronJ [2]. Data are expressed as the average number of neurites of a certain length per cell as mean ± SEM. At least 200 cells were analyzed per condition to allow statistical analysis and images were collected from 4 independent samples.

Determination of cell doubling time and cell cycle phase distribution. Quantitative determination of cell doubling times occurred through manual cell counting using a Bürker chamber. C17.2 cells were seeded at $2*10^5$ cells/flask in 25 cm² tissue culture flasks and allowed to settle overnight. Then, media were aspirated and cells were incubated with fresh media containing the QDots at 0, 2 or 10 nM for 24 h. Then, media were removed, cells washed three times with PBS, lifted by 0.25% Trypsin (Gibco, Invitrogen, Belgium) and reseeded in 25 cm² tissue culture falcons at $2*10^5$ cells/flask for every condition. Then, cells were kept in culture for 72 h after which the number of cells were counted and the cell doubling times were determined for every condition. Data are expressed as mean ± SEM for 5 independent experiments. Please note that following QDot incubation, the cells were lifted by Trypsin and reseeded at a fixed density of live cells (Trypan blue negative) in order to counter any possible loss of cells due to minor cytotoxic effects and hereby relating any observed differences in cell numbers directly to alterations in cell cycle kinetics.

For quantitative analysis of cell cycle, C17.2 cells were seeded at $2*10^5$ cells/flask in 25 cm² tissue culture flasks and allowed to settle overnight. Then, media were aspirated and cells were incubated with fresh media containing the QDots at 0, 2 or 10 nM for 24 h. Then, media were removed, cells washed three times with PBS, lifted by 0.25% Trypsin and reseeded in 25 cm² tissue culture falcons at $2*10^5$ cells/dish for every condition. Then, cells were kept in culture for 48 h after which the cells were lifted by Trypsin, pelleted and stained for nuclear DNA using the Nuclear ID Green Cell Cycle analysis kit, according to the manufacturer's protocol. Samples were then analyzed using a 5-color FACS Calibur (Becton Dickinson, Erembodegem, Belgium). For quantification all experiments were performed in triplicate and 10,000 events were collected for every sample. The samples were illuminated with an Argon laser (488 nm) and fluorescence emission was measured in the FL1 channel equipped with a

530/30 nm bandpass filter. Analysis was performed using WinMDI 2.9 where the respective cell cycle phases for every condition were calculated using 20 spectra of a total of 5 independent experiments.

Using this approach, the inhibition of cell cycle progression of C17.2 and PC12 cells by incubation of 60 µM Apigenin was also assessed. After 2 days of exposure of either cell type with 60 µM Apigenin, a clear shift of cells from G1 into G2 phase was apparent, which is to be expected for Apigenin which acts as an inhibitor of G2/M cell cycle progression. An exemplary FACS histogram is shown in Supplementary Figure S15.

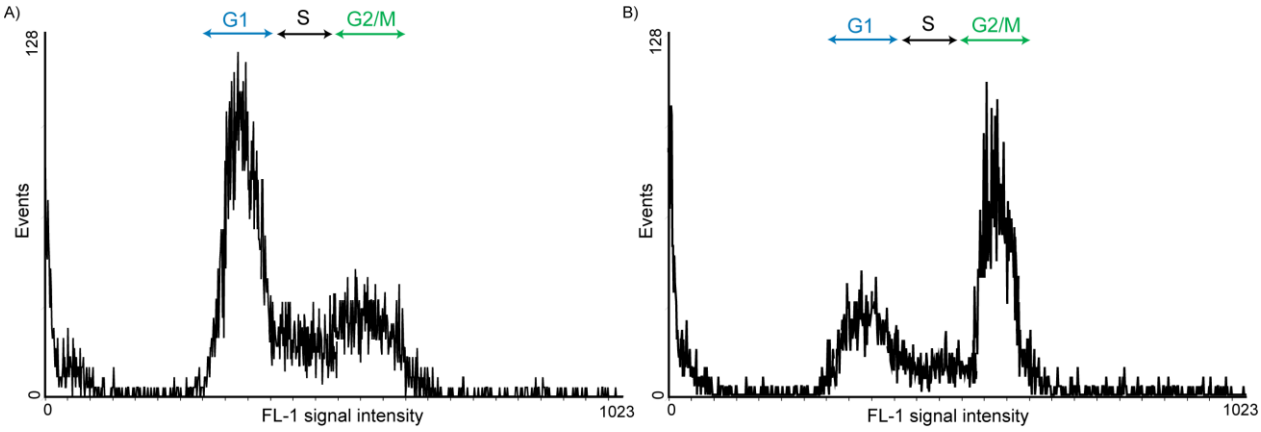

Supplementary Figure S15. Cell cycle progression status for proliferating and proliferation-restricted C17.2 cells. Flow cytometric profile of the cellular DNA levels for **A)** C17.2 in normal culture conditions and **B)** C17.2 cells treated with 60 µM Apigenin for 2 days.

Determination of QDot transfer in proliferating cells. Qualititative analysis of cell cycle progression occurred by incorporation of 5-ethynyl-2'-deoxyuridine (EdU) with the Click-iT EdU Cell Proliferation Assay Kit (Molecular Probes, Invitrogen, Belgium). To this end, C17.2 cells were seeded at $1*10^4$ cells/dish in collagen-coated 35 mm diameter glass bottom MatTek dishes or in 25 cm² tissue culture flasks at $1*10^5$ cells/flask and allowed to settle overnight after which the cells were incubated with the carboxy-QDots at 0, 0.5 or 1 nM for 24 h. Cell numbers were kept sufficiently low on purpose to enable cellular proliferation without any inhibition due to cell-cell contact. Following incubation, media were aspirated, cells washed twice with PBS and the cells seeded in the MatTek dishes received fresh medium containing 10 µM EdU after which the cells were further cultured for 18 h. The cells seeded in the 25 cm² dishes were given fresh medium and kept in culture, where for half of the dishes, cells were reseeded in MatTek dishes at $2.5*10^4$ cells/dish and $1*10^5$ cells/flask every other day

either at the odd or even days after QDot exposure. The cells reseeded in the flasks were kept in culture for 2 more days and then treated similarly for the duration of the experiment (a total of 7 days), where the MatTek seeded cells were allowed to settle overnight and then incubated with 10 μM Edu for 18 h. This time point was selected as being slightly less than the normal cell doubling time of the cells, to allow approximately all cells in the population to progress through the S phase of cell division and hereby incorporate EdU, a thymidine analog. Prior to analysis, media were removed, cells washed three times with PBS, fixed in 2% PFA for 20 min at ambient temperature, permeabilized in 0.1% Triton X-100 for 15 min at ambient temperature and then stained for the presence of EdU with Alexa Fluor 488-azide, according to the manufacturer's protocol. Cell nuclei were then also counterstained using DAPI (300 nM; 5 min) after which the dishes were stored at 4°C until being viewed by epifluorescence microscopy (Nikon Cs1).

The number of EdU positive cells was determined by analyzing the microscopy images using ImageJ, where data are expressed as mean $\pm$ SEM for 3 independent experiments. From the collected images, more than 250 cells/condition out of 3 independent experiments were analyzed for the number of EdU-positive nuclei relative to the total number of DAPI-stained nuclei.

The number of QDot positive cells were analyzed similarly, where images obtained from 3 independent experiments were analyzed using ImageJ. Data are expressed as mean $\pm$ SEM and are gathered by more than 250 cells analyzed per condition. Data are given as the number of QDot positive cells over the total number of DAPI-stained cells.

The number of QDot clusters per cell was determined as described above in the section entitled "Quantitative determination of cellular QDot levels".

The number of cells with more than 5 QDot clusters which were also positive for EdU were determined by first determining and selecting the number of cells with more than 5 QDot clusters using ImageJ. For these cells, the number of EdU positive nuclei over the total number of DAPI-stained nuclei was determined as described above. Data are expressed as mean $\pm$ SEM for 3 independent experiments.

Determination of secondary ROS effects. As ROS can result in DNA damage, the occurrence of DNA double strand breaks was determined by staining C17.2 cells for γ-H_2Ax.

Cells were seeded in collagen-coated 35 mm diameter glass bottom MatTek dishes at $5*10^4$ cells/dish in 1.5 ml of full culture medium. Cells were allowed to settle overnight prior to being incubated with either type of QDots for 24 h at 0, 2, 10 or 20 nM. Next, medium was removed, cells were washed twice with PBS and fresh medium without any particles was given and cells were kept in culture for an additional 24 h. Then cells were washed three times with PBS, fixed in 2% PFA for 20 min at ambient temperature, permeabilized with 1% Triton X-100 for 15 min at ambient temperature and blocked with 10% goat serum-containing PBS for 30 min. The cells were then incubated with primary rabbit anti-γ-H_2Ax antibody (1 µg/ml; Abcam, Cambridge, UK) for 2 h followed by 1 h incubation with Alexa Fluor 488-conjugated goat anti-rabbit antibody (1/250; Molecular Probes, Invitrogen, Merelbeke, Belgium) at ambient temperature. To get quantitative data, the fluorescence intensity level for γ-H_2Ax on the images was determined using ImageJ (NIH, USA) for 200 cells per condition based on images taken from at least 4 different samples/condition. The values are expressed relative to the control level (= 100%) as mean $\pm$ SEM.

For determination of the mitochondrial membrane potential ($\Delta\Psi_m$) C17.2 cells were seeded at $2*10^4$ cells/well in black 96 well plates and allowed to settle overnight. Cells were then incubated with either type of QDots at 0, 2, 10 or 20 nM for 24 h after which the medium was removed and cells were incubated for 30 min with 20 µM of JC-10 (Enzo Life Sciences, Zandhoven, Belgium) at 37°C. Next, cells were washed 3 times with PBS and the plate was measured using a Wallac Envision plate reader with an excitation filter of 480 nm and emission filters of 520 and 590 nm. The data are expressed as the ratio of green (damaged mitochondria) over red (healthy mitochondria) fluorescence as mean $\pm$ SEM (n = 3).

Cellular calcium levels were determined using the Fluo-4 Direct Calcium Assay Kits (Molecular Probes, Invitrogen, Merelbeke, Belgium). C17.2 cells were C17.2 cells were seeded at $2*10^4$ cells/well in black 96 well plates and allowed to settle overnight. Cells were then incubated with either type of QDots at 0, 2, 10 or 20 nM for 24 h after which the medium was supplemented with the Fluo-4 reagent for 30 min at 37°C and 2 h at ambient temperature according to the manufacturer's protocols. Next, the plate was measured using a Wallac Envision plate reader with an excitation filter of 490 nm and emission filter of 520 nm. The data are expressed as mean $\pm$ SEM for 3 independent experiments.

Statistical analysis. All data are expressed as mean ± SEM unless indicated otherwise and data were analyzed using one-way analysis of variance (ANOVA). Multiple comparisons were analyzed using the Tukey- (honestly significant difference test) post-hoc method. When comparing the different NPs to the same control group (the reference group), the Dunnett post-hoc analysis method was used. In all cases, the degree of significance is indicated when appropriate (* : $p < 0.05$; ** : $p < 0.01$; *** : $p < 0.001$).

Supplementary references.

[1] Soenen SJ, Himmelreich U, Nuytten N, Pisanic TR, 2nd, Ferrari A, De Cuyper M. Intracellular nanoparticle coating stability determines nanoparticle diagnostics efficacy and cell functionality. Small 2010;6:2136-45.

[2] Meijering E, Jacob M, Sarria JC, Steiner P, Hirling H, Unser M. Design and validation of a tool for neurite tracing and analysis in fluorescence microscopy images. Cytometry A 2004;58:167-76.